AFIT/GAE/ENY/93D-28

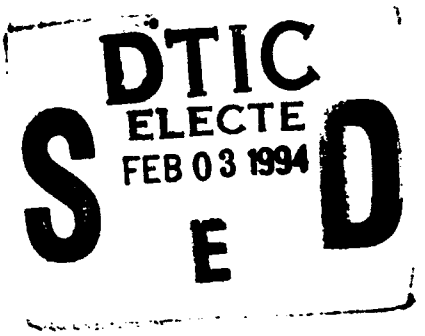

FATIGUE BEHAVIOR OF A CROSS-PLY CERAMIC MATRIX COMPOSITE AT ELEVATED TEMPERATURES UNDER TENSION-TENSION LOADING

THESIS

Richard J. Tuznik
Captain, USAF
AFIT/GAE/ENY/93D-28

Approved for public release; distribution unlimited

The views expressed in this thesis are those of the author and do not reflect the official policy or position of the Department of Defense or the U.S. Government.

AFIT/GAE/ENY/93D-28

FATIGUE BEHAVIOR OF A CROSS-PLY CERAMIC MATRIX COMPOSITE AT ELEVATED TEMPERATURES UNDER TENSION-TENSION LOADING

THESIS

Presented to the Faculty of the Graduate School of
Engineering of the Air Force Institute of Technology
Air University
In Partial Fulfillment of the
Requirements for the Degree of
Master of Science in Mechanical Engineering

Richard J. Tuznik
Captain, USAF

December 1993

Acknowledgements

I would like to express my gratitude to my advisor, Dr. Shankar Mall, for his guidance throughout my graduate program and this project. My thanks also go to Dr. Anthony Palazotto and Captain Robert Canfield for serving on my graduate committee. I would also like to thank Dr. Walter Jones, of AFOSR/NA, for sponsoring this research.

I must also acknowledge the AFIT laboratory personnel for their fine efforts in maintaining the lab facilities. I especially want to thank Mark Derriso for keeping my test station in working order, and Dan Rioux for his many hours spent modifying the scanning electron microscope.

My wife, Cynthia A. Tuznik, provided moral support and encouraged me to always keep the end goal in sight. Her patience, thoughtfulness, and love will always be remembered.

Finally, special appreciation is due my children, Jessica L. Tuznik and Ian S. Tuznik, for their love and understanding.

Table of Contents

List of Figures and Tables

Table #

Abstract

The purpose of this study was to investigate the behavior of Nicalon/Calcium-Aluminosilicate (Nicalon/CAS), cross-ply, $[0/90]_{2S}$, ceramic matrix composite at elevated temperatures under tension-tension fatigue loading. The primary objective of this study was to investigate the different damage mechanisms involved at the elevated temperatures and their effects on the fatigue life of this material.

Ultimate tensile strength tests and tension-tension fatigue tests were conducted at room temperature (RT), 700° C, and 850° C. The average values of the initial elastic modulus in tension were 121 GPa at RT, 118 GPa at 700° C, and 107 GPa at 850° C. The ultimate strengths were 275, 153, and 119 MPa respectively.

Tension-tension fatigue tests with a load ratio of R = 0.10 and a frequency of 10 Hertz were run at 700° C and 850° C. Results from a previous study conducted at RT using maximum stresses of 180, 160, and 140 MPa with cycles to failure of 1,609, 50,443, and 1,000,000 (cycle run out) respectively were analyzed. At 700° C, tests were accomplished at maximum stresses of 110, 83, and 69 MPa with cycles to failure of 20, 3,767, and 1,000,000 respectively. At 850° C, tests were accomplished at maximum stresses of 85, 55, 52, and 50 MPa with cycles to failure of 510, 360,

1,000,000, and 1,000,000 respectively. Finally, two interrupted tension-tension tests were run, one at 700° C and one at 850° C, where acetate edge replicas were taken to monitor crack growth.

Damage behavior was investigated using fatigue life curves, normalized modulus results, maximum and minimum strain data, crack densities, and post-mortem fractographic specimen evaluation.

Analysis of these results showed identical damage behavior at RT and 700° C. Ultimate failure was caused by an accumulation of matrix damage, most of which occurred on the first cycle. However, at 850° C, significantly less damage occurred to the matrix. Fiber debonding was the major damage mechanism responsible for final failure at this elevated temperature.

FATIGUE BEHAVIOR OF A CROSS-PLY CERAMIC MATRIX COMPOSITE AT ELEVATED TEMPERATURES UNDER TENSION-TENSION LOADING

I. Introduction

A. Background

As technology continues to grow at an ever increasing rate, better materials will be needed to meet engineering uses in the future. As an example, the Air Force is actively involved in attempts to increase the thrust to weight ratio of the current turbine engines. Another Air Force goal is to advance its aerospace vehicles from supersonic to hypersonic flight. Both of these, and many other projects, require strong, light weight materials capable of withstanding cyclic loads at high temperatures [1].

One class of material currently being studied to solve these design problems is the ceramic matrix composite. Ceramics have long been known for their strength and resilience in high temperature environments. However, their structural uses are severely limited by a lack of toughness and ductility.

With new manufacturing techniques, toughness and ductility are significantly increased by adding reinforcement, such as fibers, to a ceramic matrix. This develop-

ment of toughened ceramics during the past 15 years is undoubtedly one of the most important breakthroughs of this century in the field of material science [2].

In general, ceramic matrix composites exhibit high damage tolerance before catastrophic failure due to their less brittle failure characteristics with the presence of reinforcing fibers. Toughness is imparted in the ceramic matrix composites by a range of mechanisms at the micro-scale. These mechanisms are (1) matrix cracking, (2) fiber/matrix debonding, (3) fiber sliding, (4) fiber breakage, and (5) fiber pull-out [3]. Each ceramic matrix composite material exhibits unique stress-strain behavior based on the progression of these five failure mechanisms.

Existing failure theories to model or account the toughening mechanisms of ceramic matrix composites are generally based on a weak fiber matrix interface, leading to transverse microcracking, followed by fiber pull-out and final failure. There is experimental evidence to justify these mechanisms. However, most of these results are limited to room temperature [1,3-9]. Very few of these experiments are available at high temperatures. Further, even fewer studies have focussed on fatigue behavior at elevated temperatures [10,11]. Furthermore, these studies only offer limited explanations of the fatigue damage mechanisms involved at elevated temperatures, so there is a need for more research of fatigue behavior at elevated

temperatures to determine precisely how damage progresses in ceramic matrix composites in this environment. The ability to identify and monitor useful damage parameters is required in order to characterize damage initiation and progression leading to final failure.

B. Problem Statement

The purpose of this study was to investigate the effects of tension-tension fatigue loading in a model ceramic matrix composite. For this purpose, a silicon fiber (Nicalon) reinforced calcium-aluminosilicate (CAS) ceramic matrix composite with a cross-ply lay-up was chosen. Previous studies [11,12] have shown that the damage mechanisms differ significantly at about 815° C in this ceramic matrix composite. Therefore, this study investigated and compared the damage mechanisms under tension-tension loading at three temperatures, 20° C, 700° C, and 850° C.

C. Approach

A 110 kN MTS test station was modified to include specially fabricated quartz heater lamps, water cooled grips, and heat containment shields. Simulated tests were conducted to show that the test set-up could withstand a temperature up to 1200° C for 30 hours while remaining within the operating limits of the MTS machine.

A Nicalon/CAS ceramic composite plate was cut into the rectangular specimens having 153.0 mm length and 5.1 mm width. End tabs of a soft aluminum were applied to the ends of the specimens with a resin epoxy.

Static tension tests were performed at elevated temperatures to determine ultimate tensile strengths at the three selected temperatures. Next, tension-tension fatigue tests were performed to determine the applied stress versus fatigue life relationship, S-N curves, and the threshold at which cycle run out (of one million cycles) occurred for each temperature. Finally, a tension-tension fatigue test was run at each elevated temperature which was stopped at each decade to take an acetate edge replica of the loaded specimen to document the history of damage initiation and progression.

Load and displacement data were recorded logarithmically for fatigue tests at cycles 1,10,100,..., 1,000,000. Material behavior and damage was recorded by four primary methods: stress-strain curves, elastic modulus, hysteretic energy densities, and acetate edge replication techniques.

Elastic modulus measurements were made from each stress-strain curve. The unloading portion of the curve was used to calculate the modulus. Change in the modulus with respect to the number of cycles, which indicated material damage during fatigue loading, was investigated. Hysteretic energy dissipated during a fatigue cycle was

calculated from the area under the stress-strain curves which was calculated using the trapezoid rule to yield an energy/volume value. These energy values indicated the damage incurred by the material during cycling.

A systematic investigation of damage mechanisms was made by using each of the above methods. These results were compared with existing room temperature results obtained by Opalski [8] and a previous study by Rousseau at elevated temperature [11] to explain the effects of elevated temperatures on the tension-tension fatigue behavior of the tested model ceramic matrix composite.

II. Background

For ceramic composite materials to be of a real engineering value for the application in engines and airframe structures, there must be an accurate knowledge of their behavior under high temperature cyclic loads. However, because this field is in its infancy, only limited fatigue studies have been documented. Also, the failure mechanisms during fatigue are not yet fully understood [2].

Zawada Butkus and Hartman [1] performed fatigue tests on a silicon carbide fiber reinforced aluminosilicate glass in order to better understand the nature of damage accumulation during cycling. They concluded that for a cross-ply material to accumulate enough damage for failure before a million cycles, it must be fatigued at a stress level above the proportional limit of the material. This proportional limit was defined as the value at which non-linear stress-strain behavior begins due to the onset of microcracking of the matrix during static loading. They also noted that matrix cracks in the transverse plies significantly decreased the modulus during cycling, but had a little effect to predict fatigue life. Also, they observed the phenomenon of modulus increase during the latter portions of fatigue tests and offered several possible explanations based on interfacial sliding friction, damage

accumulation, and interaction of fatigue produced debris with the still intact fiber-matrix system.

Zawada, Pernot, and Butkus [9] examined parameters that influence high cycle fatigue life. They studied four types of ceramic matrix composites using various combinations of three matrix materials and two types of fibers. Each ceramic matrix composite exhibited unique behavior under cyclic loading. Fatigue damage accumulated at a different rate for each system tested. They concluded that each ceramic matrix composite exhibited unique tensile stress-strain behavior depending on the fiber-matrix architecture. They found no clear trend to predict fatigue limits based on static strengths of the fibers, matrix, or architecture. However, they did identify the fiber as the dominant parameter that controls the fatigue limit in ceramic matrix composites under ambient conditions.

Kuo and Chou [7] examined the damage evolution of a Nicalon cross-ply composite using shear lag models and an energy balance method. They found closed form solutions for two ideal cases: perfect bonding of the fibers to the matrix and fiber/matrix interface sliding. These ideal cases have limited use for engineering applications since environmental factors are ignored.

Holmes [13] pointed out that significant environmental factors include the effects of humidity increasing interfacial shear stiffness between the fiber and the

matrix at room temperature and oxidation of the carbon at the fiber/matrix interface at elevated temperatures. In particular, at elevated temperatures, the oxidation of the carbon at the fiber/matrix interface can significantly reduce the fatigue life of the Nicalon fibers.

Butkus, Zawada, and Hartman [10] performed fatigue tests on unidirectional Nicalon reinforced aluminosilicate glass (SiC/1723) specimens at elevated temperatures. They observed that at 800° C the fracture surface showed two distinct failure mechanisms. The specimen developed a deep embrittled zone at all four exposed outer surfaces. This embrittled zone failed in a flat fracture manner, while the interior material showed a jagged surface.

Rousseau [11] conducted a preliminary investigation of mechanical behavior for Nicalon/CAS cross ply laminate at 20° C and 815° C. He observed significant damage after the first load cycle in the form of cracks in the transverse matrix plies at both temperatures. He also observed that the fatigue lives of specimens tested at 815° C were much shorter than the fatigue lives of specimens tested at 20° C. He attributed this to fiber/matrix interfacial embrittlement brought on by exposure of the Nicalon fibers to the high temperature air as a result of the matrix cracking.

III. Experimental Procedure

All experiments for this study were conducted in the Aeronautics and Astronautics Laboratory at the Air Force Institute of Technology, located at Wright-Patterson Air Force Base in Dayton, Ohio. Many of the procedures used in performing these tests were similar to previous theses completed at the Air Force Institute of Technology and from research methods presently in use at the Air Force Materials Laboratory [1,8,9,14], also located at Wright-Patterson Air Force Base, so that test results of the present study could be directly compared to other research efforts.

A. Test Set-Up

The test set-up consisted of six major components: 1) a materials test stand, 2) rigid hydraulic grips, 3) a control console, 4) heating lamps, 5) a refrigeration unit and heat deflector shields, and 6) a personal computer.

The basic material test station was the MTS Systems Corporation Materials Test Station, Model No. 318.10. It had a maximum force capability of 100 kN through the integral hydraulic actuator. The test stand was aligned during initial installation and recently checked by the technician before testing for this project began.

MTS Systems Corporation hydraulic wedge grips, Model No. 647.02, were used. These rigid grips were modified to include internal channels for coolant to flow through them during high temperature testing. The maximum allowable operating temperature of the grips was 177° C. The maximum temperature that the cooled grips reached during high temperature testing was 89° C.

An MTS Systems Corporation 458.20 Microconsole was used to control the test stand. A 9 kN load card was used in a DC Control Module, Model No. 458.11, to provide stress control for the tests. The load card was calibrated by a contracted maintenance technician before any actual testing was done. An AC Controller Module, Model No. 458.13, with a 12.7 cm displacement card was used to provide additional control of the integral actuator.

The specimens were heated by two locally designed and fabricated lamps using quartz bulbs. Two bulbs were used in each lamp, and the lamps were positioned on opposite sides of the specimen during testing. Specimen temperature was monitored with K type thermocouples attached to the specimen surface. The output of the heat lamps was controlled independently by Barber Colman, Model No. 560, temperature controllers.

A refrigerated recirculation unit, Neslab HX-75, was the heart of the closed loop cooling system. It supplied continuously cooled water to the heat lamp assemblies, heat

shields, extensometer mount, and grips. The heat shields were locally designed and fabricated, and mounted to both grips. These shields limited the high temperature zone to the immediate area of the specimen.

A Zenith 386 personal computer was used to employ the High Cycle Fatigue software package, MATE 233, that controlled the tests.

B. Specimen Background and Preparation

The material tested in this study was a silicon fiber (Nicalon) reinforced calcium aluminosilicate ceramic matrix composite. Ceramic matrix composites are generally formed by a two stage process. These stages consist of passing a fiber tow through a slurry tank (containing the matrix powder, binder, and carrier liquid), winding it on a drum, and then allowing it to dry. Next, the tows are cut and stacked and hot pressed at temperatures above 1200° C to minimize porosity [15].

Nicalon is an amorphous/crystalline fiber, predominantly silicon carbide, made by the Nippon Carbon Company. It is approximately 15 micron in diameter, and commonly available in an 1800 denier tow. The matrix was a calcium-aluminosilicate crystalline glass-ceramic made by Corning Glass. The actual plate used in this study was a 15.3 cm square plate with a $[0/90]_{2S}$ lay-up. The individual plies were approximately 0.40 mm thick and consisted of about forty percent fiber by volume [8].

The plate was cut into specimens, 5.1 mm wide and 153.0 mm long, using a Buehler high speed saw with a diamond wafering blade. After the specimens were cut, they were inspected visually for cracks or chips that may have been caused by the cutting process. None sustained any noticeable damage.

One edge of approximately three-fourths of the specimens length was, then, polished for each test that would require edge replicas and/or photographs to investigate damage mechanisms. The polishing process involved using a Buehler Polimet I Polisher and various Buehler grinding and polishing products. Initial grinding involved using a disk impregnated with 30 micron diamond chips. After approximately 15 minutes at 200 rpm, the surface had a uniform grainy appearance and was ready for the next step. Next, the same procedure was followed using a disk impregnated with 12 micron diamond chips, and finally with a disk impregnated with 6 micron diamond chips. This completed the grinding portion of the polishing process and produced a surface that was free of large voids when viewed under a microscope at a magnification of 100. If large voids were still present, the above three grinding procedures were repeated.

Lapping was the next step of the polishing procedure. A nylon cloth was attached to the Polimet I wheel. Diamond suspension pastes and fluids of the following grades were

successively used to polish each specimen: 9 micron, 6 micron, 3 micron, and 1 micron. The final surface clearly showed the transverse fibers, and a minimum of voids.

The final step in specimen preparation was to attach end tabs to each specimen. A soft aluminum, 2020-0, was chosen for the end tabs. The end tabs were 2.5 cm long, 0.6 cm wide, and 1.6 mm thick. Four tabs were attached to each specimen using epoxy resin as shown in Figure 1.

C. Experimental Procedure

Each test began by preparing a specimen for application of the thermocouples. Marks using silver paint were applied 1.3 cm above and below the center of the specimen. The area between these marks was the gage length of the specimen. A 0.6 cm wide band of masking tape was then wrapped around the specimen and covered each of these paint marks. Then, another 0.6 cm band of masking tape was applied 0.5 cm away and towards the edge from each of the existing bands of masking tape as shown in Figure 1. The exposed 0.5 cm zones between the paired bands of masking tape were the regions where the thermocouples were later attached to the specimen.

Before mounting the specimen in the MTS machine, a specimen level fixture specifically designed for this test, as shown in Figure 2, was calibrated against the integral actuator of the MTS machine. This calibration was done by first raising the integral actuator to the approximate test

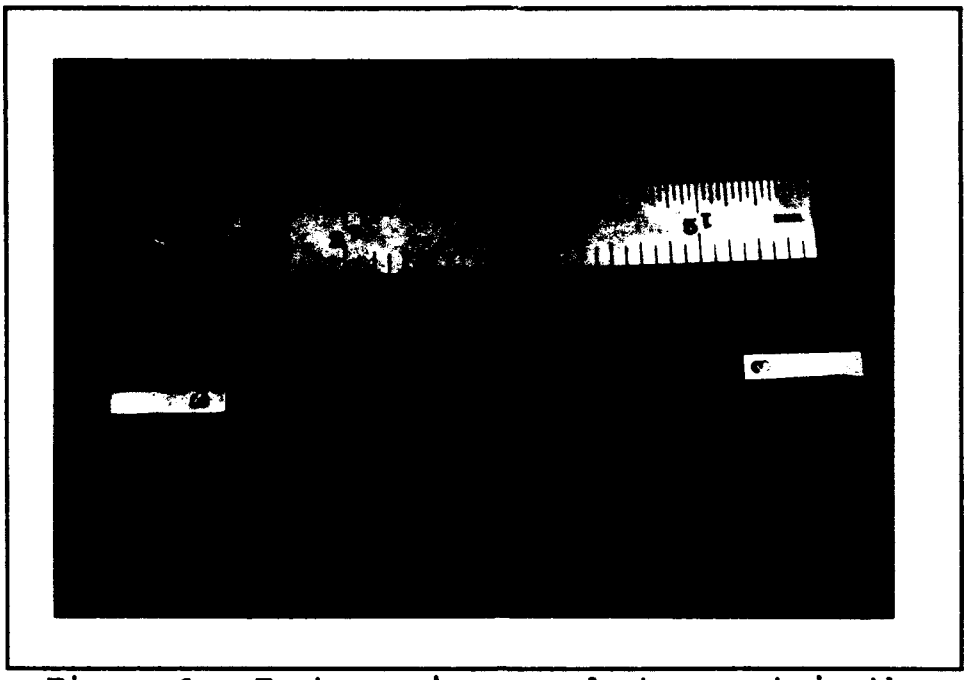

Figure 1. Test specimen ready to mount in the MTS machine.

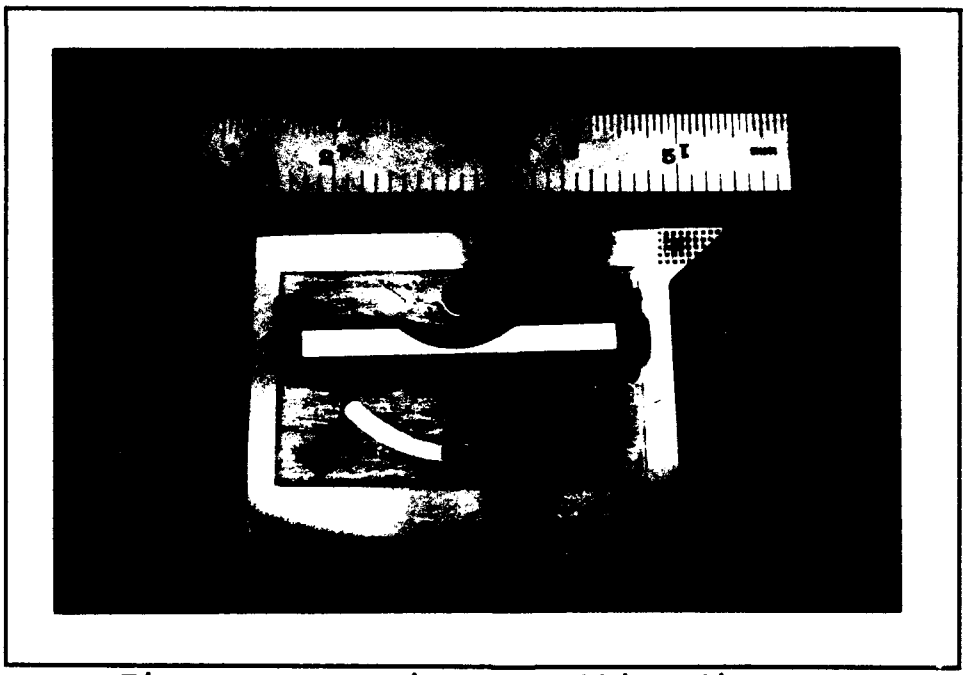

Figure 2. Specimen levelling fixture.

position. Then, the specimen level fixture was pressed against the actuator and the rotating bubble level indicator was adjusted so that the bubble was between the level marks as shown in Figure 3. Finally, the bubble level indicator was locked into position by tightening the set screws. This completed the calibration of the levelling fixture and the integral actuator was returned to its maximum displacement position.

The specimen was then mounted to the calibrated specimen level fixture using two rubber bands. The top of the specimen was positioned in the top grip, hydraulic grip pressure was adjusted to 5 MPa, and applied to the top grip as shown in Figure 4. The specimen was then checked to ensure that it was in alignment with the stroke of the integral actuator and that the entire aluminum end tab was in the grip.

The next step was to attach the thermocouples to the specimen. A 36 gage strand of alumel wire was passed through the loop created by welding the K type thermocouple. The thermocouple was then temporarily attached to the specimen with a strip of masking tape, while the ends of the alumel strand were loosely twisted together until the strand held the thermocouple in place. Then, the strip of masking tape was removed and the alumel strand was tightened so that the thermocouple bead was held firmly against the specimen, while not creating a short

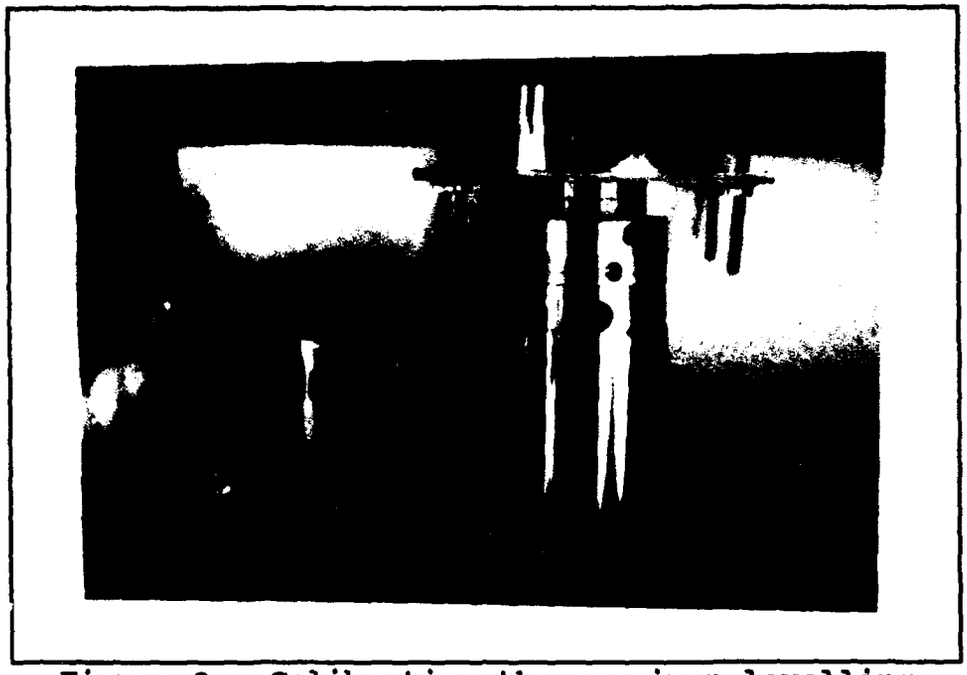

Figure 3. Calibrating the specimen levelling fixture.

Figure 4. Mounting a test specimen in the MTS machine.

circuit across the thermocouple junction. A thermocouple properly secured to a specimen is shown in Figure 5. Then, 903 Green Ceramic Adhesive was applied around the specimen between the bands of masking tape until the thermocouple junction and alumel wire were completely covered as shown in Figure 6. The masking tape bands were then removed from the specimen.

The next step was to cure the ceramic adhesive. The refrigerated recirculation system was turned on, along with the cooling air. The quartz heat lamps were positioned approximately 8 cm away from the specimen. The MATE software was then programmed to heat the specimen to 120° C for 2 hours.

After curing the ceramic adhesive, it was the time to warm-up the hydraulics system of the MTS machine for the actual test. The high pressure hydraulics was activated with the MTS Microconsole. Using the MATE Utilities software, the MTS integral actuator was cycled with a 10 Hertz triangular shaped input wave. The span control of the displacement controller was adjusted for approximately 3 cm of total travel of the integral actuator. This warm-up run lasted a minimum of 10 minutes prior to each test.

Following the MTS machine warm-up run, control of the integral actuator was switched from the displacement control module to the load control module. Then the bottom

grip was carefully moved into place and attached to the lower end of the specimen and adjusted for zero load.

After both ends of the specimen were mounted in the grips with zero load applied, the quartz rod extensometer was positioned on the specimen as shown in Figure 7. Only a moderate amount of pressure was required to hold the quartz rod in place. This kept induced bending stresses in the specimen as small as possible.

Finally, each heat lamp was positioned approximately one cm from either side of the specimen and the MATE software was programmed to run an actual test. A specimen ready to begin a test is shown in Figure 8. To keep the test procedures as consistent as possible, a five minute ramp-up time to the test temperature was used, immediately followed by a 10 minute period of soak-up at the test temperature before the actual test began.

Three different types of tests were used to conduct this study. They were the monotonic tensile test, the high cycle fatigue test without any interruptions, and the high cycle fatigue test with interruptions to take edge replicas. The experimental procedures for each type of test are discussed below.

For the monotonic tensile tests, a stress of 30 MPa was applied two successive times to check for any slippage of the extensometer rods before the actual test began. If slippage occurred, the specimen was cooled, the extenso-

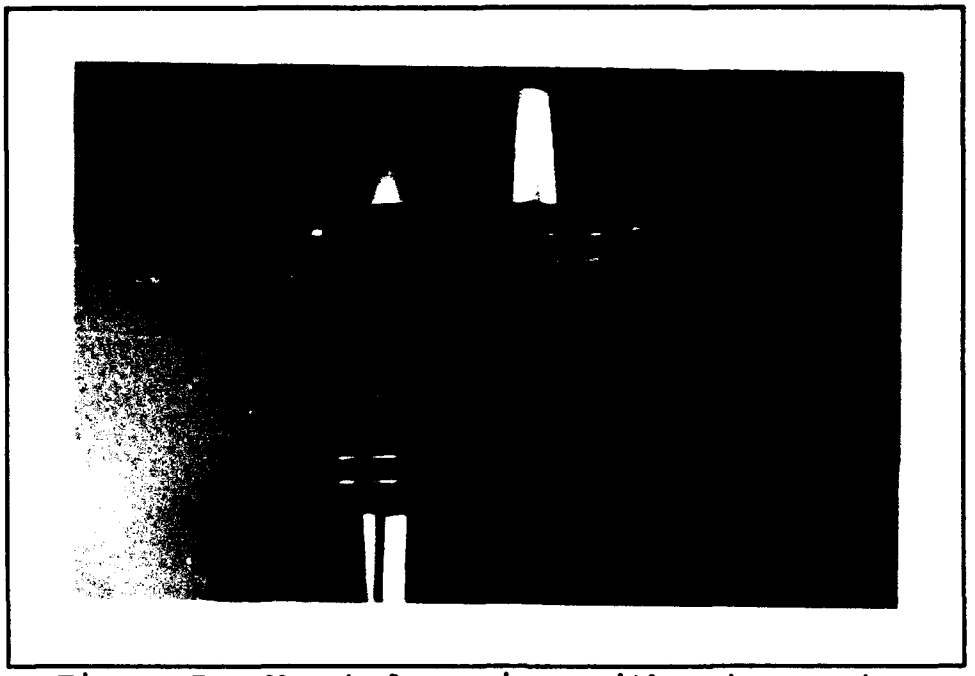

Figure 7. Mounted specimen with extensometer attached.

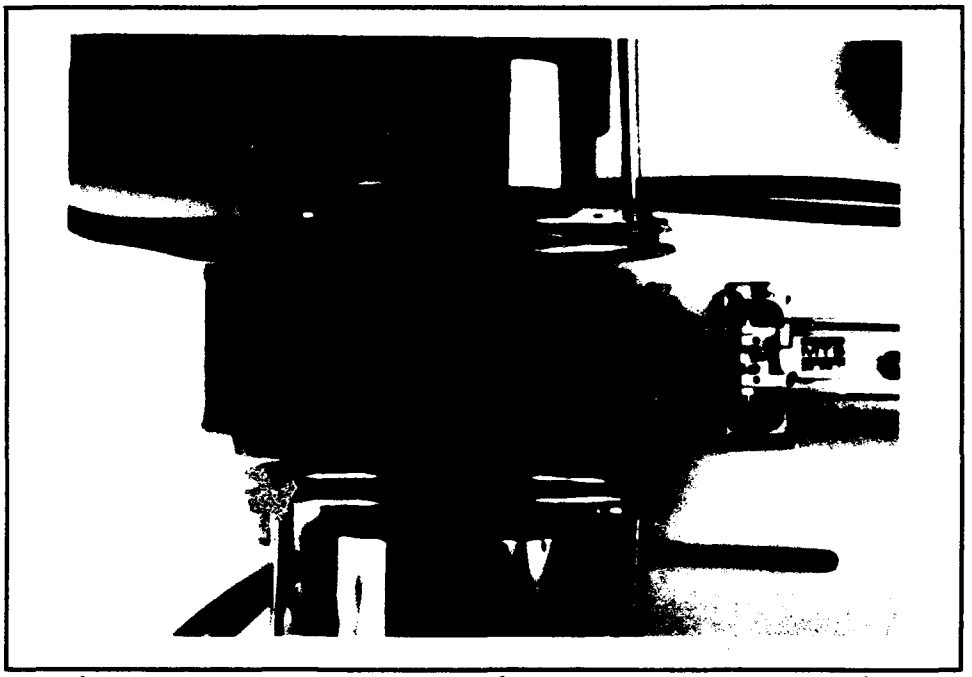

Figure 8. Mounted specimen ready for testing (front heating lamp not shown).

meter rods were adjusted appropriately, and the specimen was reheated again. If no slippage was detected, the test began and was run with a stress rate of 1.0 MPa/second until failure occurred.

For the high cycle fatigue tests, a stress of 30 MPa was applied at a rate of one Hertz for two successive cycles to check for slippage of the extensometer rods. Once it was determined that the rods would not slip during the fatigue loading, the test began. All high cycle fatigue tests were run with a load ratio of 0.10. Stress and fatigue data were logarithmically recorded during the test at 1,10,100,..., 1,000,000 cycles. The stress was controlled by a triangular input wave at 1 Hz for the first 100 cycles and 10 Hz for the remainder of each test. High cycle fatigue tests ran until the specimen experienced catastrophic failure or reached a cycle run out (arbitrarily chosen to be 1,000,000 cycles).

The high cycle fatigue tests with replicas were run in the same manner as above, but were interrupted at each decade of cycles to make an acetate edge replica of the gage length. The procedure for making an edge replica consisted of stopping the test after the appropriate cycle and allowing the specimen to cool to room temperature with no load applied. Once the specimen was at room temperature, a 22 MPa stress was manually applied to the specimen and several edge replicas were taken. The load was then

immediately removed from the specimen and the replicas were viewed under a microscope to check their quality. Once suitable replicas were made, the specimen was reheated and temperature soaked, and then the test was continued until the next decade of cycles, when the edge replication procedure was repeated, or until the specimen failed.

D. Data Collection

Fatigue data was collected logarithmically after each decade of cycles during each test. The MATE 233 High Cycle Fatigue software recorded data at a load rate of one Hertz during each data acquisition cycle (DAC). During each DAC, the applied load, along with the displacement data from the extensometer, were recorded every 0.001 second. The load data was then divided by the cross-sectional area of the specimen being tested, which converted the load data to a stress term. The displacement data was then divided by the gage length of the extensometer, which yielded the displacement in terms of strain. These results were then plotted to create stress versus strain hysterysis loops. A typical stress versus strain hysterysis loop is shown in Figure 9.

From the hysterysis loops, Youngs Modulus for each cycle was calculated. Three methods for calculating the modulus that are widely used in research are illustrated in Figure 10. One method uses the slope of the loading portion of the hysterysis loop, as shown by the line connect-

ing points A and B in Figure 10. Another method, known as the secant modulus, is calculated from the slope of the line connecting the points of maximum and minimum displacement as shown by the line connecting points C and D in Figure 10. The final method uses the slope of the unloading portion of the hysterysis loop as shown by the line connecting points E and F in Figure 10.

This study used the modulus calculated from the unloading portion of the hysterysis loops. It was decided to use this method to calculate the modulus since this was the method used in the study by Opalski [7]. This allowed a direct comparison of the modulus at the three temperatures studied. It was also observed for the hysterysis loops recorded during this study, that the three methods used to calculate the modulus had very little effect on the value of the modulus.

Strain data was also used to monitor damage for this study. Damage was evaluated using the maximum strain, minimum strain, and the strain range for each DAC recorded. The values of strain were obtained directly from the applicable hysterysis loop.

Finally, damage was also monitored by calculating the area inside the hysterysis loop, which was calculated using the computer program provided in the Appendix. This program calculated the area inside each hysterysis loop by applying the trapezoid rule.

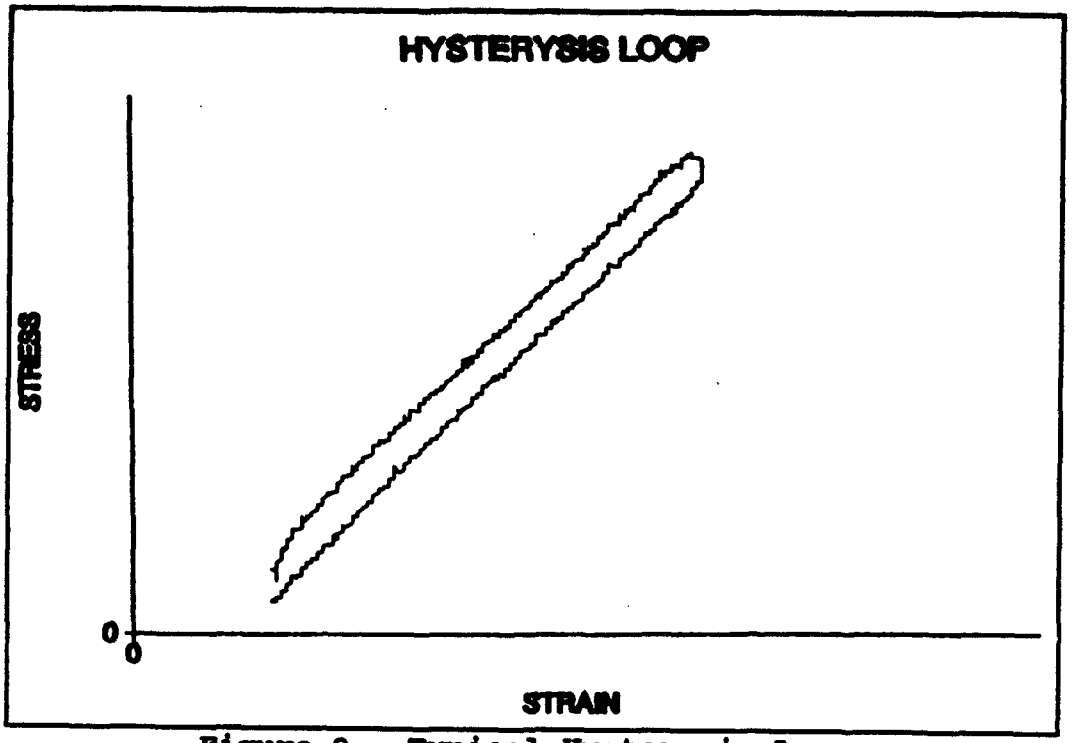

Figure 9. Typical Hysterysis Loop.

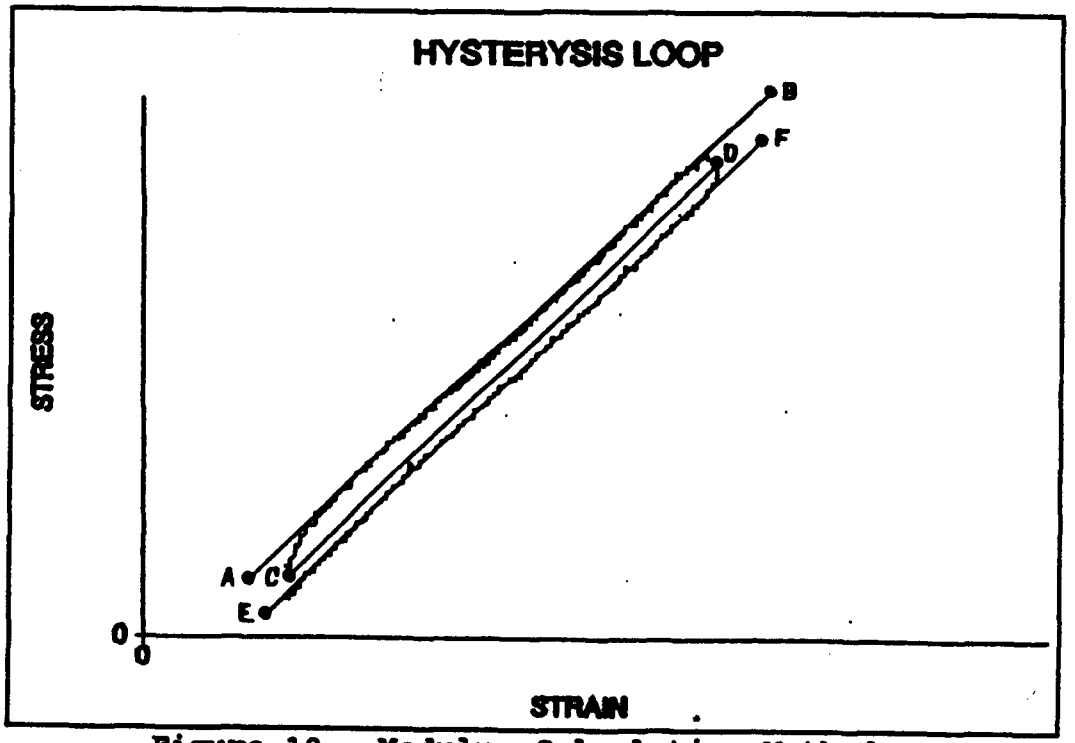

Figure 10. Modulus Calculation Methods.

Crack density results were based on analysis of acetate edge replicas accomplished after each decade of cycles during both of the interrupted tests. Cracks were counted in all of the plies along a 5.0 mm length of the specimen. The crack density was then evaluated separately for the 0° plies and the 90° plies.

Post-mortem fractographic analysis of failed specimens were performed using both optical microscopy and scanning electron microscopy. The fracture surface was investigated to determine the damage mechanisms involved in failure. The profile of the fracture surface along with the specimen edges were also investigated to determine the failure mechanisms involved.

IV. Results and Discussion

The primary purpose of this study was to investigate the fatigue behavior and damage mechanisms of a cross-ply Nicalon/CAS ceramic matrix composite at elevated temperatures. Data from both static tensile tests and tension-tension fatigue tests at room temperature (RT), 700° C, and 850° C were used for this investigation. A summary of the tests and results used for this study are shown in Table 1.

Damage mechanisms discussed in this study were observed through microscopic and macroscopic evaluations of specimens, acetate edge replicas, and post-mortem examination of specimens through scanning electron microscopy (SEM). To evaluate specimen damage, plots of the normalized modulus versus cycle count were also used as one of the means to identify damage. The normalized modulus is the modulus at any cycle divided by the initial modulus, or E/E_i.

In this chapter, Section A is a discussion of the results that were used to establish the S-N curves, and Section B is an investigation of the changes in the modulus. Section C is a comparison of the maximum and minimum strains during cycling at selected cycles. Section D is a discussion of the crack density results, Section E is a discussion of the area in the stress-strain hysterysis

Table 1. Tests and Results

SPECIMEN NUMBER	TYPE OF TEST	TEMPERATURE (°C)	MAXIMUM STRESS (MPa)	CYCLES
3*	STATIC	20	275	--
21*	STATIC	20	273	--
10*	FATIGUE	20	180	1609
7*	FATIGUE	20	160	50,433
9*	FATIGUE	20	140	10^6
1	STATIC	700	149	--
4**	STATIC	700	153	--
3	FATIGUE	700	110	20
4	FATIGUE	700	83	3767
2	FATIGUE	700	69	10^6
12	INTERRUPTED	700	73	7671
5**	STATIC	850	119	--
19	FATIGUE	850	85	510
5	FATIGUE	850	55	360
10	FATIGUE	850	52	10^6
9	FATIGUE	850	50	10^6
13	INTERRUPTED	850	53	380

* indicates this data is from Opalski's tests [8]
** indicates this data is from Agins' tests [14]

loops, and Section F is an analysis of damage based on fractographic evaluation of selected specimens.

A. Fatigue Life

Data from both tensile tests and tension-tension fatigue tests were required to establish the S-N curves. Table 1 shows that a static tensile test was performed on a test specimen at 700° C. The results from this static tensile test were identical to those obtained by Agins [14]. In order to conserve specimens, Agins' tensile test results at RT and 850° C were used in this study since specimens from that study were from the same sheet of Nicalon/CAS ceramic matrix composite as the specimens used for this study.

Tension-tension fatigue tests were performed at 700° C using a load ratio of R = 0.1 and maximum stresses of 110 MPa, 83 MPa, and 69 MPa. The test run with a maximum stress of 69 MPa was stopped after 1 million cycles, without the specimen failing.

Tension-tension fatigue tests were then performed at 850° C using a load ratio of R = 0.1 and at maximum stresses of 85 MPa, 55 MPa, 52 MPa and 50 MPa. The tests run with a maximum stress of 52 MPa and 50 MPa were stopped after 1 million cycles since specimens did not fail.

The results from the static and tension-tension fatigue tests performed at 700° C and 850° C are shown in Figure 11. Also shown in Figure 11 is an S-N plot from RT

tests. The RT data was obtained from Opalski's work previously done on the same Nicalon/CAS ceramic matrix composite with an identical cross-ply lay up [8].

Investigation of Figure 11 showed that, in general, the Nicalon/CAS cross-ply ceramic matrix composite degraded under both static tension and tension-tension fatigue conditions as the temperature was increased.

In order to compare the trends of the three fatigue life curves in Figure 11, the curves were normalized with respect to their ultimate static strengths. These normalized fatigue life curves are shown in Figure 12. Figure 12 shows that the shapes of the S-N curves at RT and 700° C are similar to each other with very little scatter, but the 850° C curve shows significant scatter between the tests conducted at 85 and 55 MPa. This difference is explained next.

It is known from previous studies [1,4,5,8,10-13,15] with cross-ply ceramic matrix composites that ultimate failure occurs when the longitudinal fibers fail. It has been previously shown in many studies that up to this point, damage accumulates at a fairly regular rate until final failure occurs. This damage is initially in the form of matrix cracks occurring in the 90° plies, which then spread to the 0° plies. Cracks then continue to grow across and through the matrix in the 0° plies until the longitudinal fibers ultimately carry the entire load. This

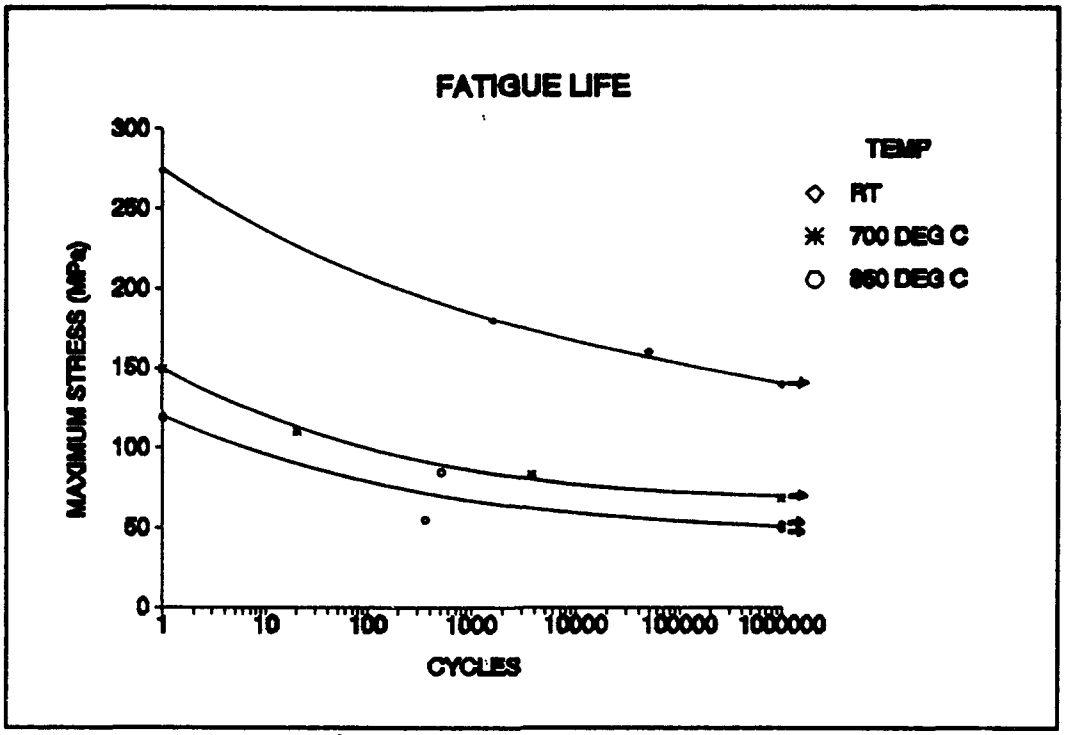

Figure 11. S-N Curves.

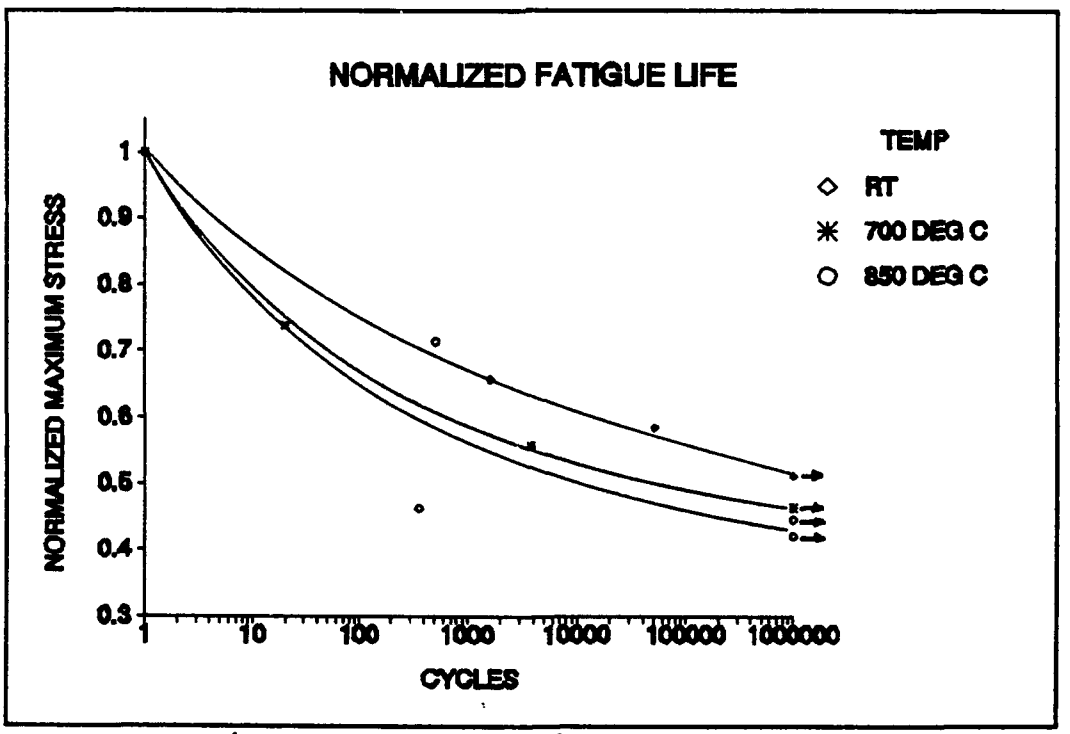

Figure 12. Normalized S-N Curves.

is shown in Figure 12 at RT and 700° C by the data forming linear S-N curves with very little scattering which indicates matrix dominated damage.

Figures 13 and 14 show the fatigue life data collected at 850° C and data from a previous study by Rousseau [11] conducted at 815° C. These S-N curves show that the specimen failed in under 500 cycles when loaded above 52 MPa, and reached cycle run out when loaded below 52 MPa. This indicates that the fibers supported the entire load after about 500 cycles, and the matrix sustained damage for only a very short period of time. A possible explanation is that soon after the matrix initially cracked and exposed the fibers to the environment, the fibers quickly began to oxidize and debonded from the matrix material. This means that less damage was allowed to build up in the matrix material over the duration of the tests conducted at 850° C. These observations will be supported further in the following sections.

B. Normalized Modulus

It has been shown in many previous studies [1,5,8,9] that the normalized modulus can be used to monitor damage progression in a cross-ply ceramic matrix composite. The normalized modulus is defined as E/E_i, the instantaneous modulus at any fatigue cycle divided by the initial modulus of the virgin material during a static tension test.

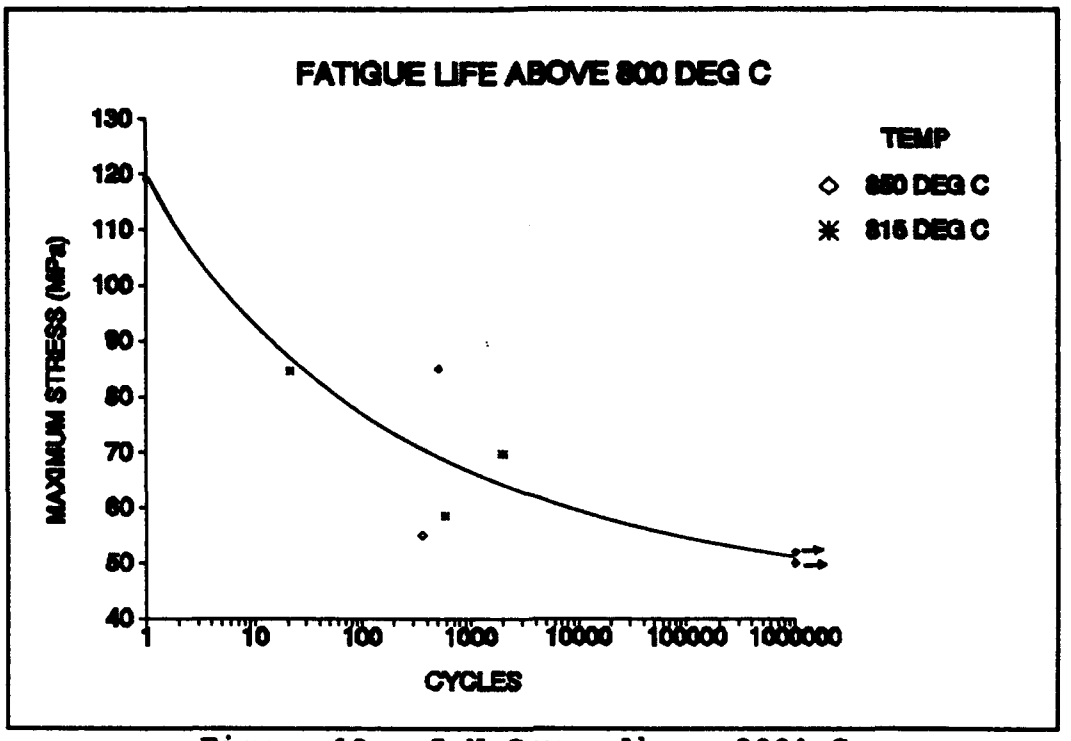

Figure 13. S-N Curve Above 800° C.

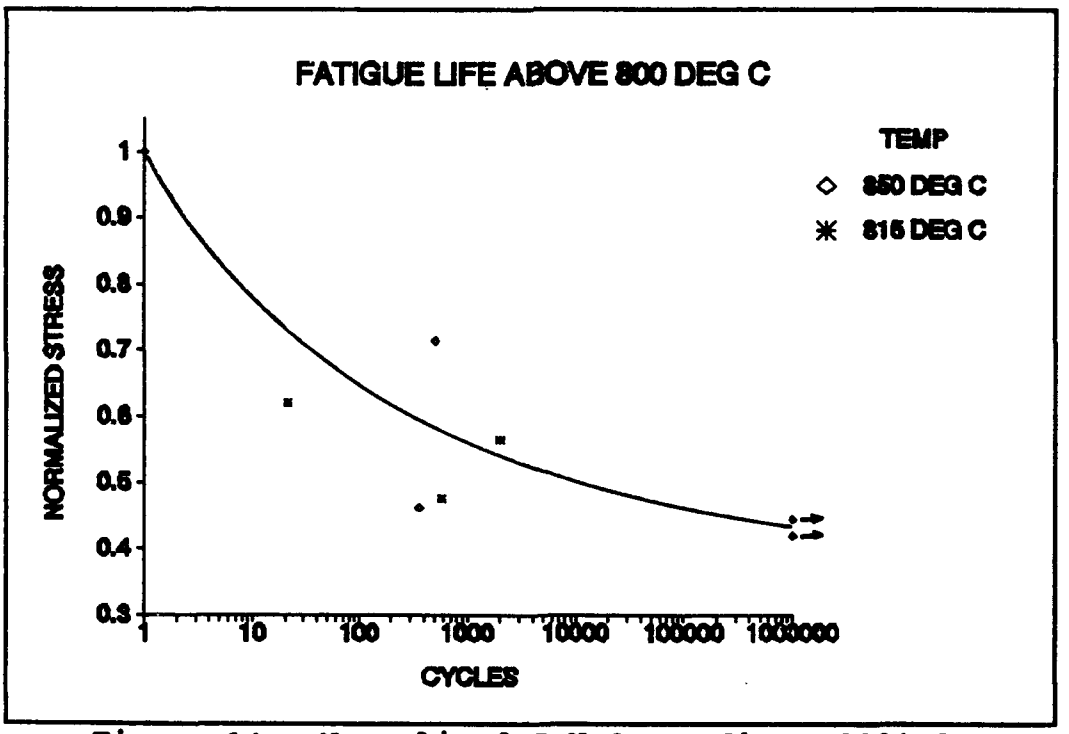

Figure 14. Normalized S-N Curve Above 800° C.

Figure 15 shows the hysterysis loops of selected fatigue cycles that were collected using the MATE 2333 High Cycle Fatigue Test software. A hysterysis loop is composed of the instantaneous stress and strain data throughout one cycle of fatigue loading. For this study, the instantaneous value of the modulus for a fatigue cycle was calculated using the slope of the linear section of the unloading portior of the appropriate hysterysis loop.

To normalize the modulus values for each cycle, the instantaneous value was divided by E_i, the initial modulus calculated from a static tensile test. Figure 16 shows the corresponding stress-strain relationship of the static tensile test that Opalski [8] conducted at RT, for the same material with the same lay-up.

Since one of the main objectives of this study is to monitor damage progression and investigate the damage mechanisms involved in tension-tension fatigue loading, the results of the tests that reached cycle run out were of the most interest. Figures 17 through 20 show the hysterysis loops and static tensile test results for tests that reached cycle run out at 700° C and 850° C respectively. These tests showed all stages of damage until the 0° fibers supported the entire load. Therefore, only these tests are discussed in detail. Results of all other tests can be found in the Appendix of this study.

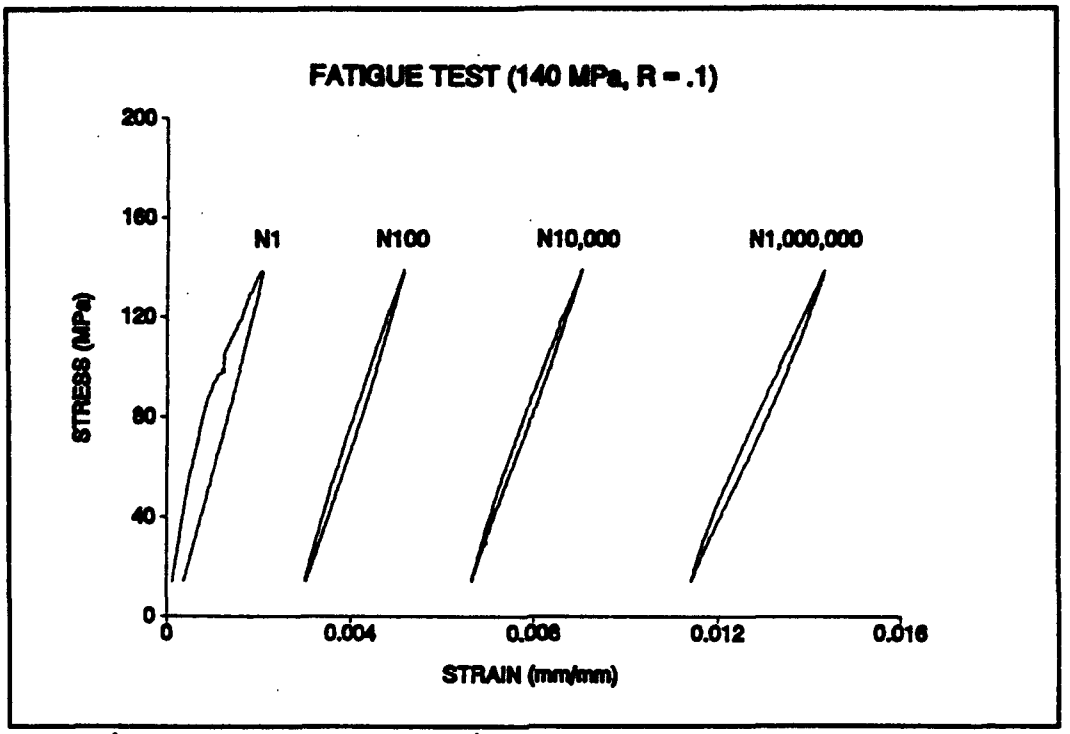

Figure 15. Hysterysis Loops, 140 MPa, RT, [8].

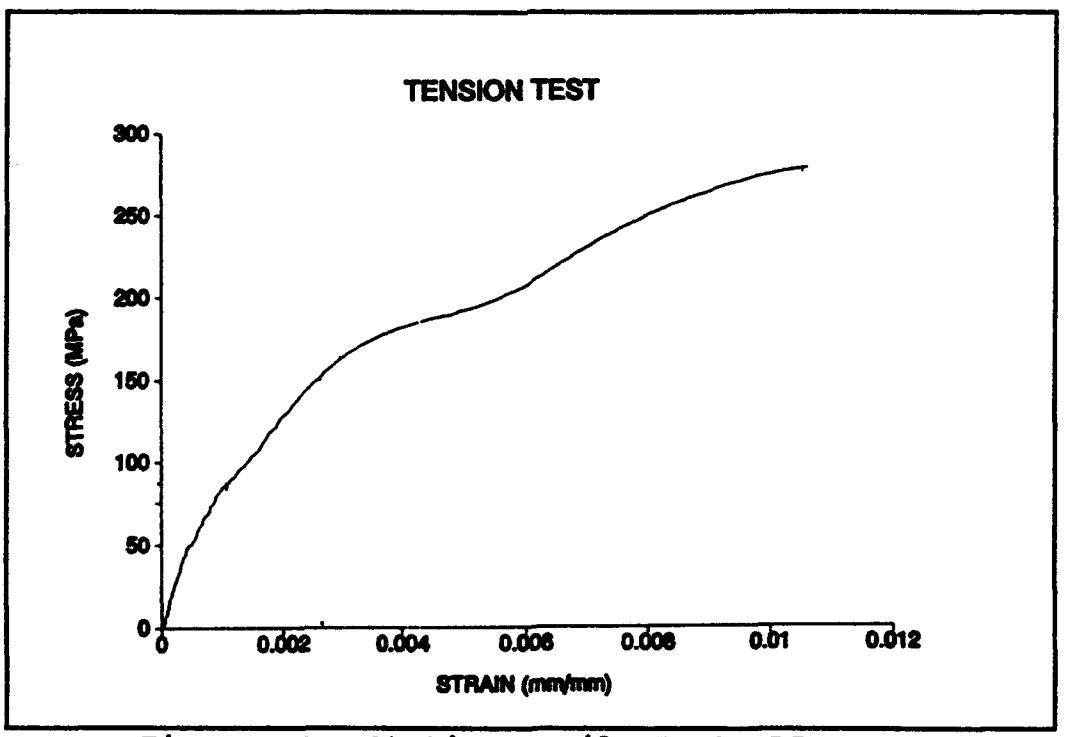

Figure 16. Static Tensile Test, RT, [8].

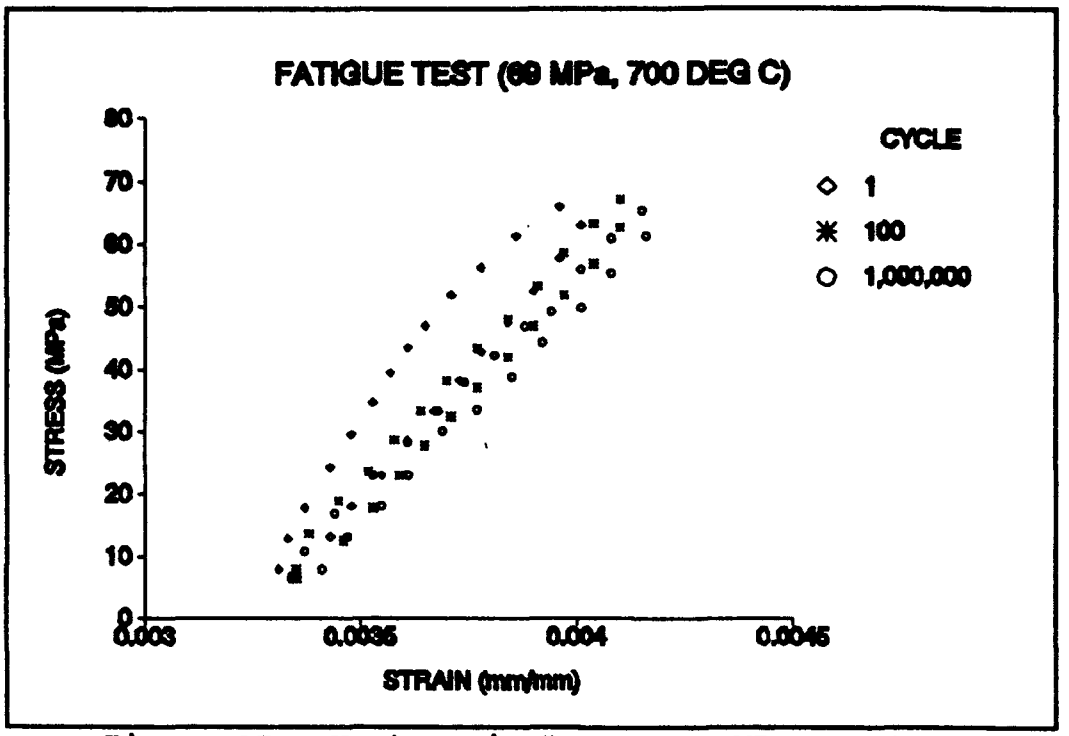

Figure 17. Hysterysis Loops, 69 MPa, 700° C.

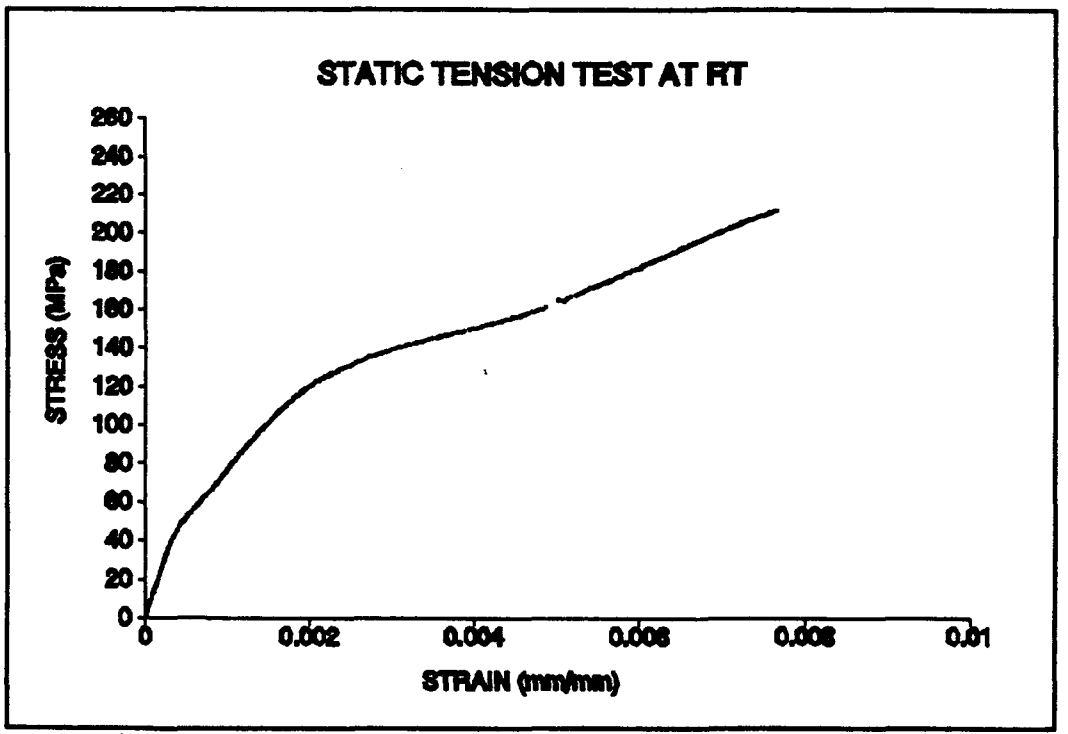

Figure 18. Static Tensile Test, 700° C, [14].

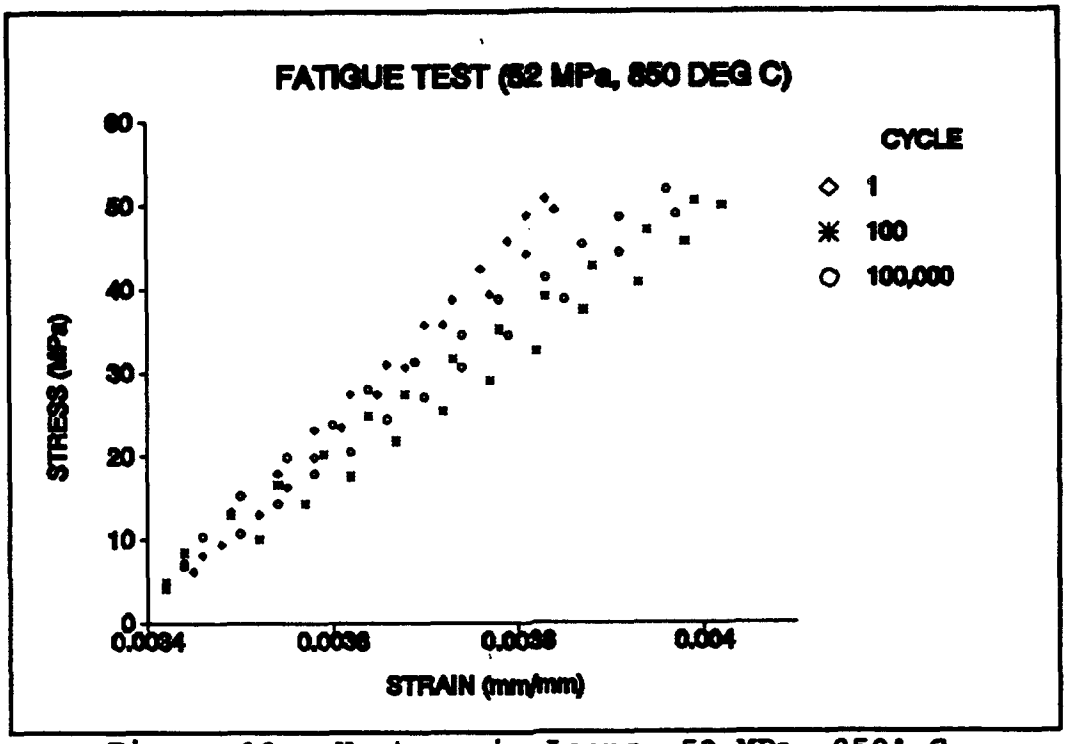

Figure 19. Hysterysis Loops, 52 MPa, 850° C.

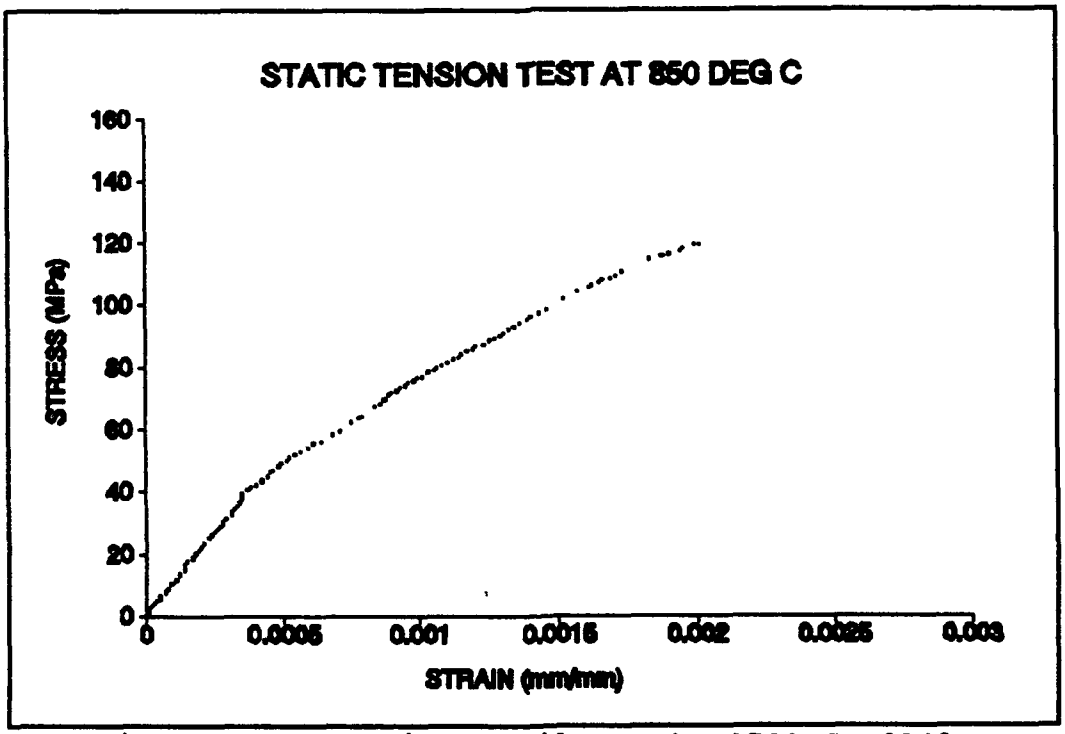

Figure 20. Static Tensile Test, 850° C, [14].

Figure 21 shows the results of the normalized modulus for the specimens that reached cycle run out at each temperature used in this study. It was shown by Opalski [8] that the normalized modulus degradation at RT over one million cycles, shown in Figure 21, was due to multiple damage mechanisms. He attributed the significant initial damage to transverse cracks initiated throughout the matrix material. This initial damage was followed by a slow and steady decrease in the normalized modulus caused by transverse cracks gradually growing through the 0° matrix. The normalized modulus then began to slightly increase at a steady rate after approximately 100,000 cycles. Opalski pointed out that this phenomenon has been explained in a previous study by Zawada [1] theorizing that debris from previous damage may have filled in the voids created by the matrix cracks and prevented full closure of these cracks after unloading.

Next, the normalized modulus degradation of the specimen tested at 700° C was compared to the specimen tested at RT. Both of these results are shown in Figure 21. The specimen tested at 700° C shows the same significant initial damage as in the RT specimen. This can be explained by the cracks initiating in the matrix material. After the initial damage, the normalized modulus slowly reduced at a steady rate. This type of behavior was also noted in the RT test. These curves show that at both RT and 700° C,

damage accumulates throughout the entire one million cycles. This accumulation of damage can be, thus, attributed to similar damage mechanisms.

However, the normalized modulus degradation curve for the specimen tested at 850° C, shown in Figure 21, is different from the RT and 700° C results. The specimen tested at 850° C did not show as much initial damage as the specimens tested at the lower temperatures. This indicated that fewer cracks were initiated in the matrix during the 850° C test. After the initial damage during the first few cycles, the normalized modulus remained relatively constant until approximately 100,000 cycles, and then began to increase. The reasons for this difference is explained next.

It was theorized by Rousseau [11] that Nicalon fibers become oxidized and stiffen at temperatures above approximately 815° C. The behavior of the specimen tested at 850° C for one million cycles strongly supports this theory. The initial damage to this specimen, shown in Figure 21, was less than the initial damage of the other two tests shown, which indicates that fewer cracks were initiated in the matrix during the first few cycles. This allowed most of the fibers to remain protected from the oxidizing environment by the matrix.

As the 850° C test continued up to approximately 100,000 cycles, the matrix cracks grew at a very slow rate,

and the effects of these cracks on the normalized modulus were negated by the fibers that were exposed to the environmental oxidizing and stiffening. Finally, after 100,000 cycles, the normalized modulus began to increase. This was caused by the exposed fibers, which were oxidized and stiffened due to the high temperature environment, fretting along their surface as they were cycled in and out of the matrix material and becoming frictionally reattached to the matrix.

Figure 22 shows the normalized modulus results for the three tests that reached cycle run out, along with the results of selected tests that failed before reaching cycle run out for each temperature investigated in this study. These results indicated that similar mechanisms were responsible for the damage that resulted in the specimens up to final failure and cycle run out at each temperature.

Figures 23 through 25 show the variation of normalized modulus as the function of fatigue cycle for all the fatigue tests performed at each temperature separately. For the specimens that failed before cycle run out at RT and 700° C, it was observed that the modulus immediately before failure was below 60% of the initial modulus. However, for the tests performed at 850° C, the modulus never dropped below 70% of the initial modulus during either test. This difference in the modulus behavior of the failed specimens is explained next.

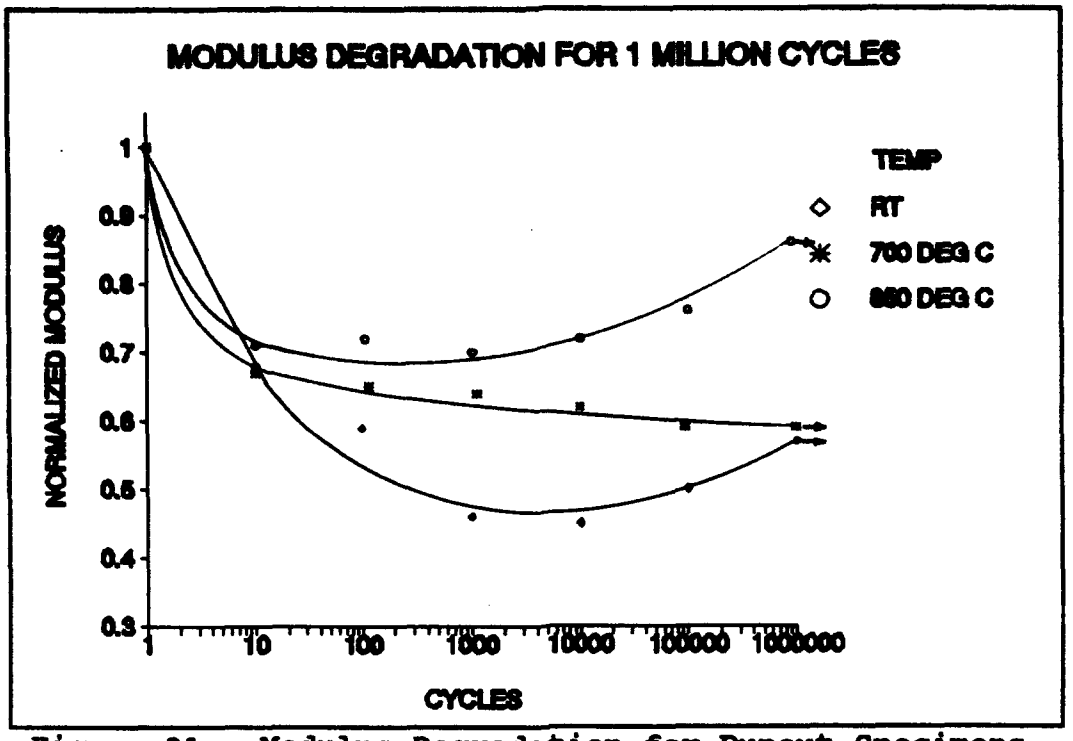

Figure 21. Modulus Degradation for Runout Specimens.

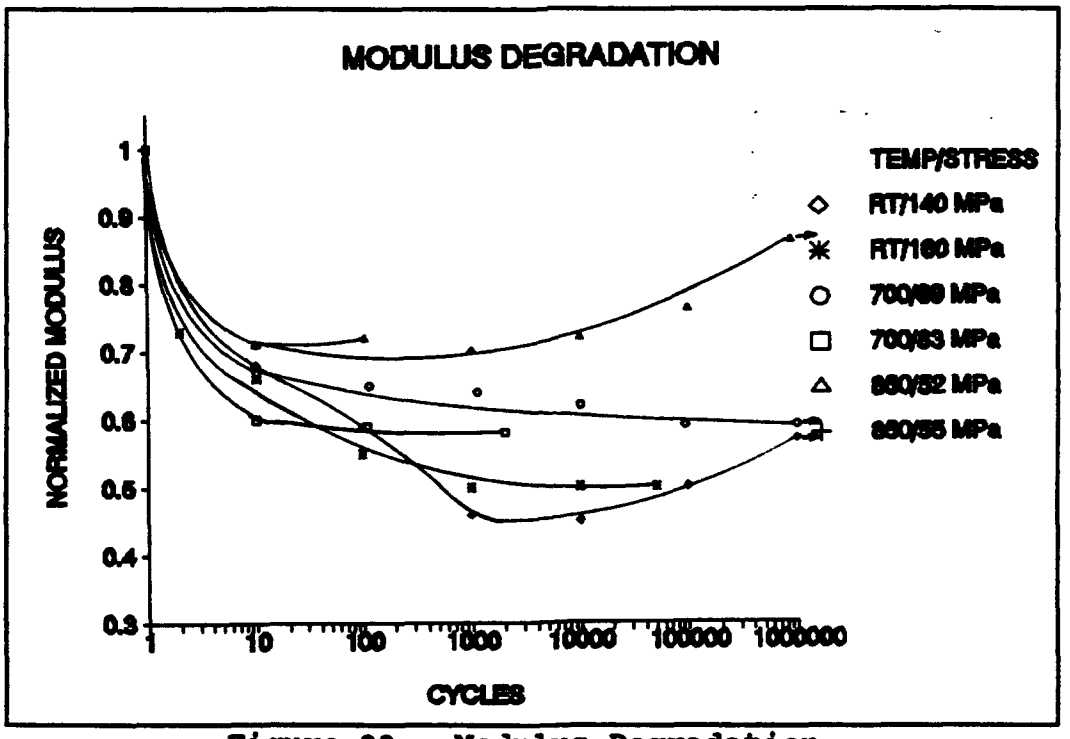

Figure 22. Modulus Degradation.

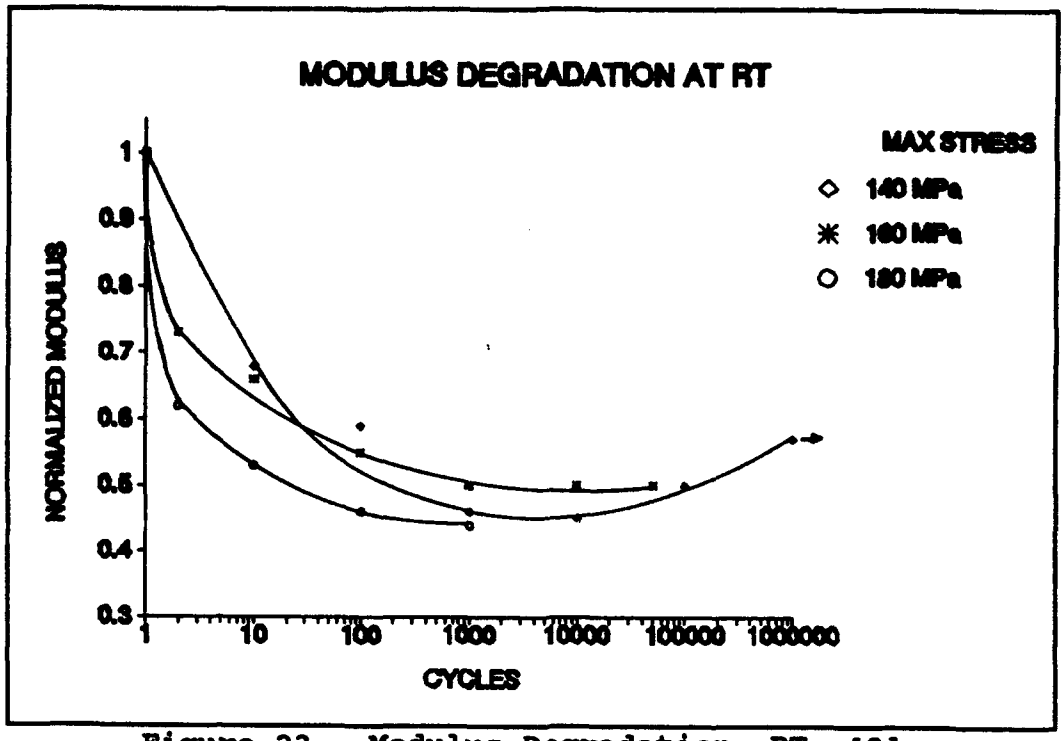

Figure 23. Modulus Degradation, RT, [8].

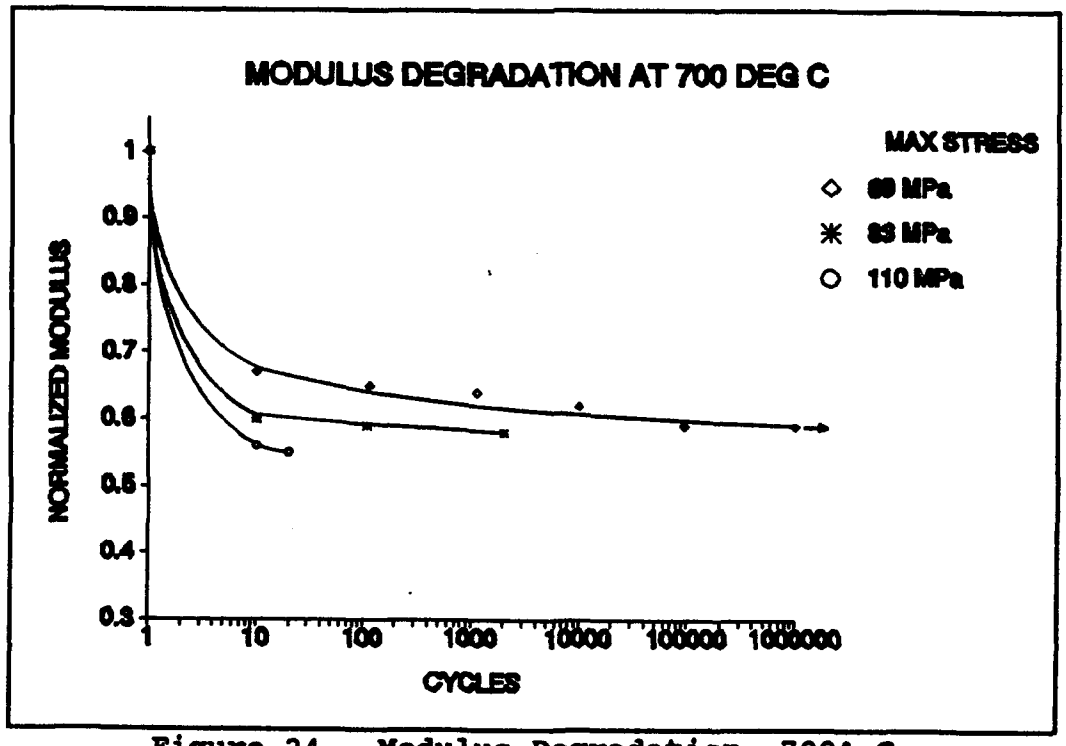

Figure 24. Modulus Degradation, 700° C.

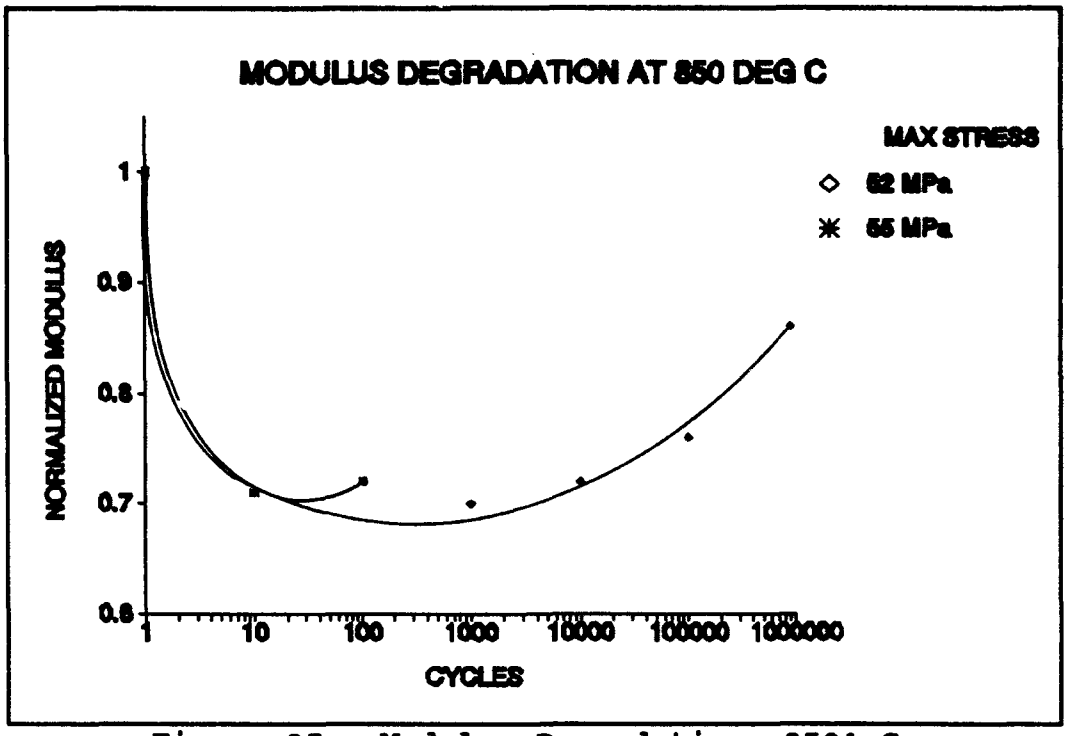

Figure 25. Modulus Degradation, 850° C.

It was shown by Opalski [8] that for the Nicalon/CAS cross-ply ceramic matrix composite, the total discount method yields a value of 61.3% when the 90° plies are assumed to have failed totally. This means that once the normalized modulus drops to a value of approximately 61% of the initial modulus, the 90° plies are cracked so extensively that they no longer are able to support any of the applied load.

For the RT and 700° C specimens which failed before one million cycles, as shown in Figures 23 and 24, the 90° plies sustained so much damage that the load was totally supported by the 0° plies after the first few cycles. This

supports the theory that gradual damage accumulated as transverse cracks grew through the 0° matrix until ultimate failure of the 0° fibers.

However, Figure 25 shows that for the specimen that failed at 850° C, the normalized modulus never went below 70%. This indicated that when the specimen failed at 850° C, the 90° plies were still able to support a portion of the applied load. This shows that damage was occurring to the fibers before the 90° plies sustained the maximum amount of damage. This can be explained by the 0° fibers being exposed to the environment and oxidized through microcracks in the 0° plies. These fibers then became brittle, which ultimately resulted in a rapid failure of the specimen.

C. Strain Data

Another way to monitor damage is by examining the maximum and minimum strain behavior during a cycle. This data was obtained from the stress-strain relationships recorded during tests. Since the normalized modulus was also extracted from these relationships, similar conclusions regarding damage mechanisms were expected.

Figures 26 through 28 show the maximum strain, minimum strain and the strain range results respectively for all the tests conducted by Opalski [8] at RT. Figure 26 shows that the maximum strain increased throughout each of these tests. Figure 27 shows the minimum strain, in general, did

not decrease throughout the tests. This supports Zawada's theory, as discussed earlier in Section B, which stated that matrix debris formed during the fatigue loading would not allow the cracks in the matrix to close completely. Figure 28 shows the strain range during each of the RT tests. These, in general, remained relatively constant throughout these tests.

Figures 29 through 31 show the results of the strain versus cycles for the tests conducted at 700° C. These figures show that the maximum strain and minimum strain both increased throughout all of the tests conducted at 700° C, and the strain range remained relatively constant. These results exhibited the same trends as the RT test results, which indicated once again that the same damage mechanisms were involved at both RT and 700° C.

Figures 32 through 34 show the results of the strain versus cycles for the tests conducted at 850° C. It was observed that for the test conducted at 850° C that reached cycle run out, Figure 32 shows the maximum strain increased during the first few cycles and then decreased for the remainder of the test. Figures 33 and 34 show that the minimum strain and the strain range both remained relatively constant throughout the tests.

Figure 35 compares the maximum strain versus cycles over one million cycles for the specimens tested at three temperatures that reached cycle run out. The maximum

strain increased throughout the tests performed at RT and 700° C. This supports the theory that similar damage mechanisms were involved at both of these temperatures. Even though the maximum strain increased at a much higher rate at RT, the strain also increased at 700° C, as shown in Figure 36, which indicated that damage to the matrix material accumulated over the entire duration of both tests.

However, the maximum strain of the specimen tested at 850° C decreased after only 10 cycles, as shown in Figure 36. This difference in behavior, as compared to the lower temperature tests, was due to the number of stiffer oxidized fibers increasing over time and eventually becoming frictionally reattached to the matrix material.

Figure 37 compares the minimum strain versus cycles over one million cycles for the three specimens that reached cycle run out. It was observed that the minimum strain increased throughout the tests performed at RT and 700° C. This was expected, based on Zawada's theory of matrix debris accumulating and not allowing cracks in the matrix to close completely. However, the minimum strain of the specimen tested at 850° C remained relatively constant throughout the test. This can be explained by recalling the discussion in Section B of this chapter which stated that the load used on this specimen created significantly

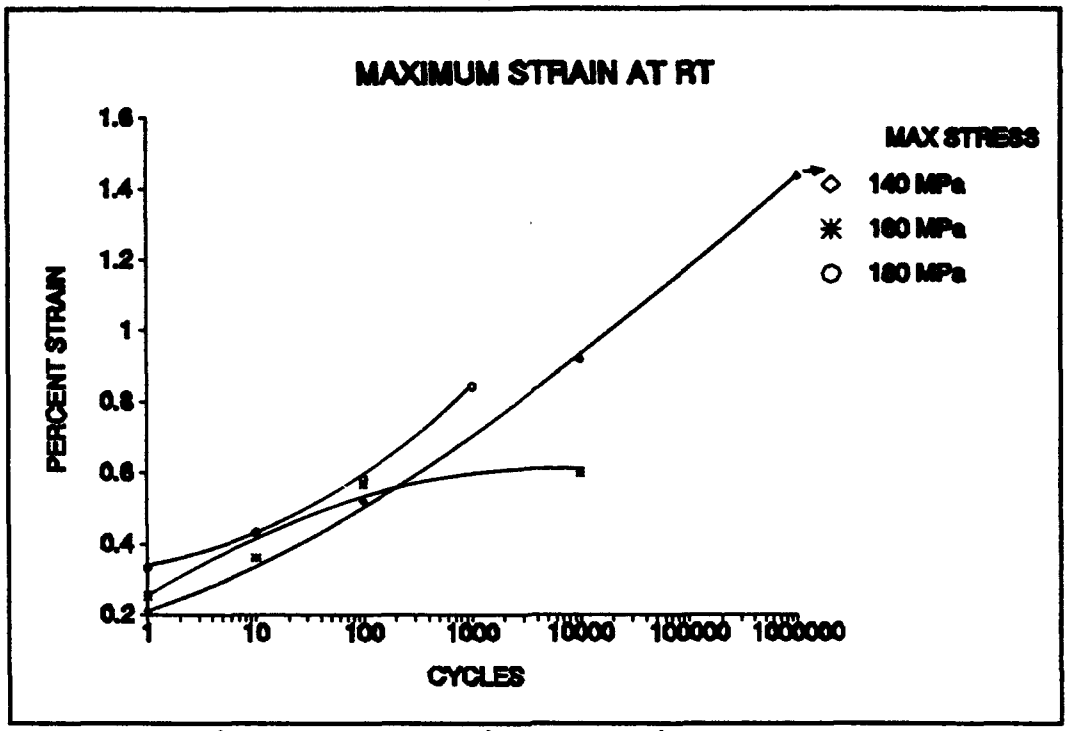

Figure 26. Maximum Strain, RT, [8].

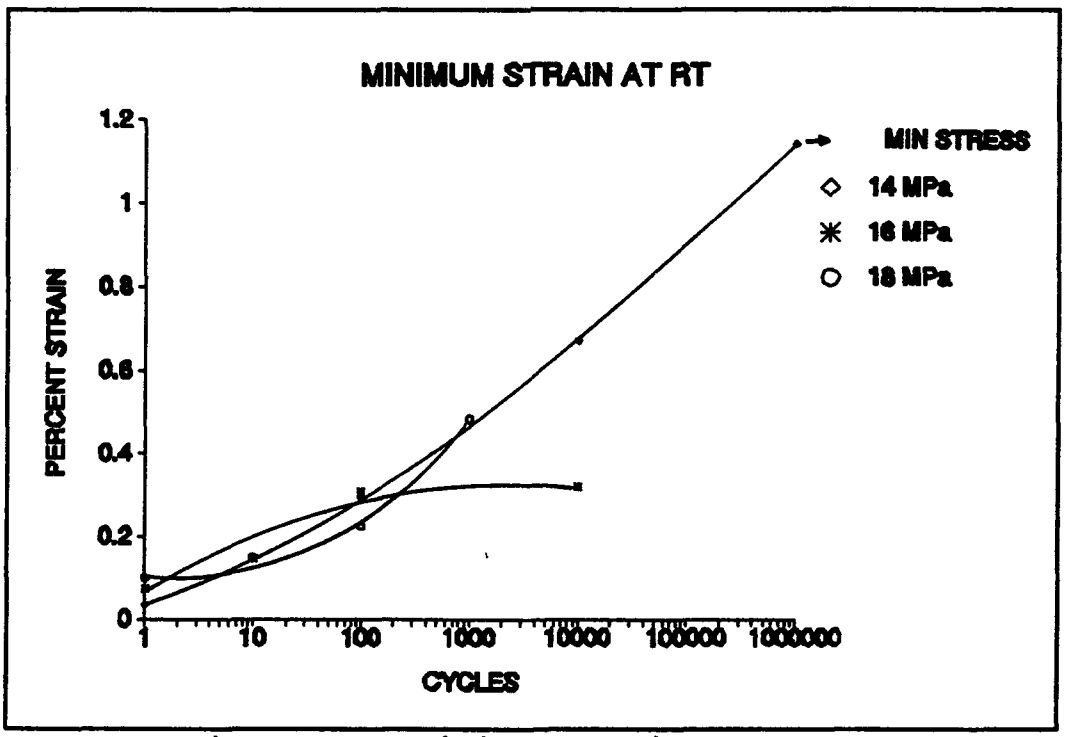

Figure 27. Minimum Strain, RT, [8].

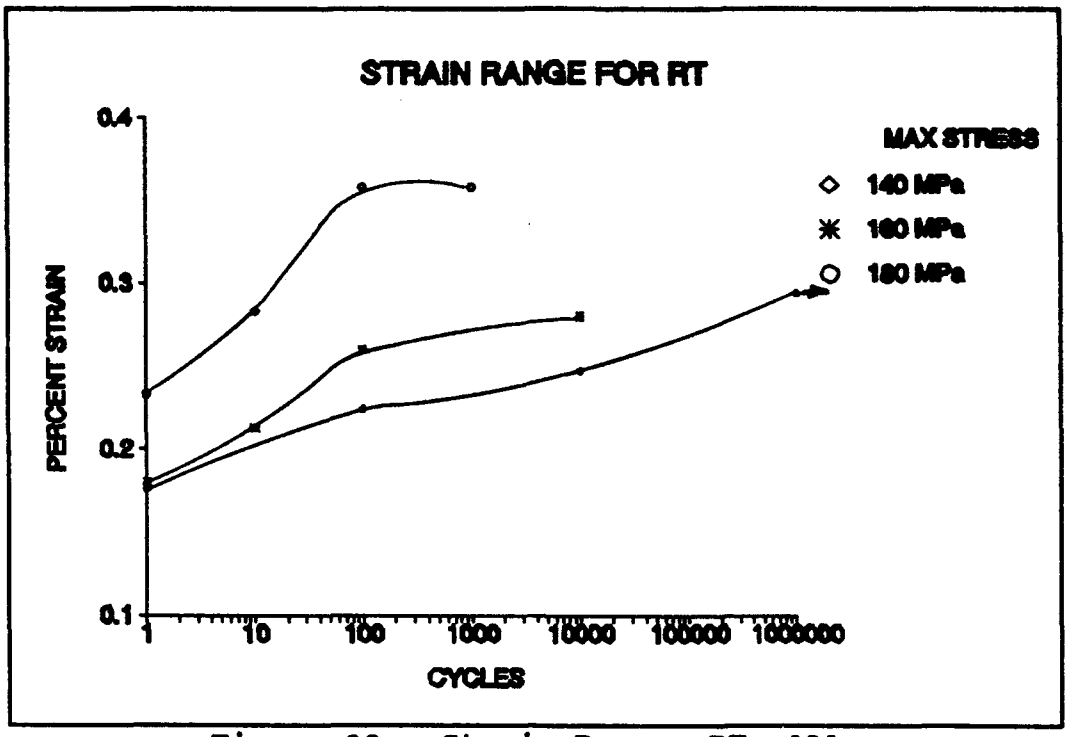

Figure 28. Strain Range, RT, [8].

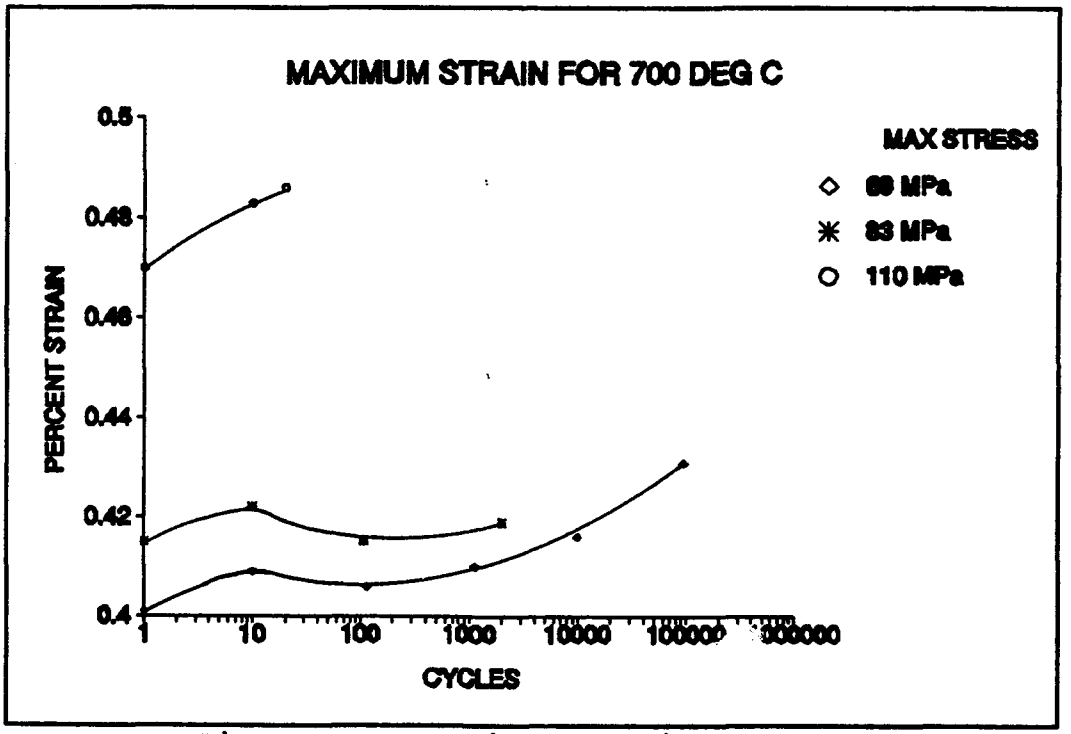

Figure 29. Maximum Strain, 700° C.

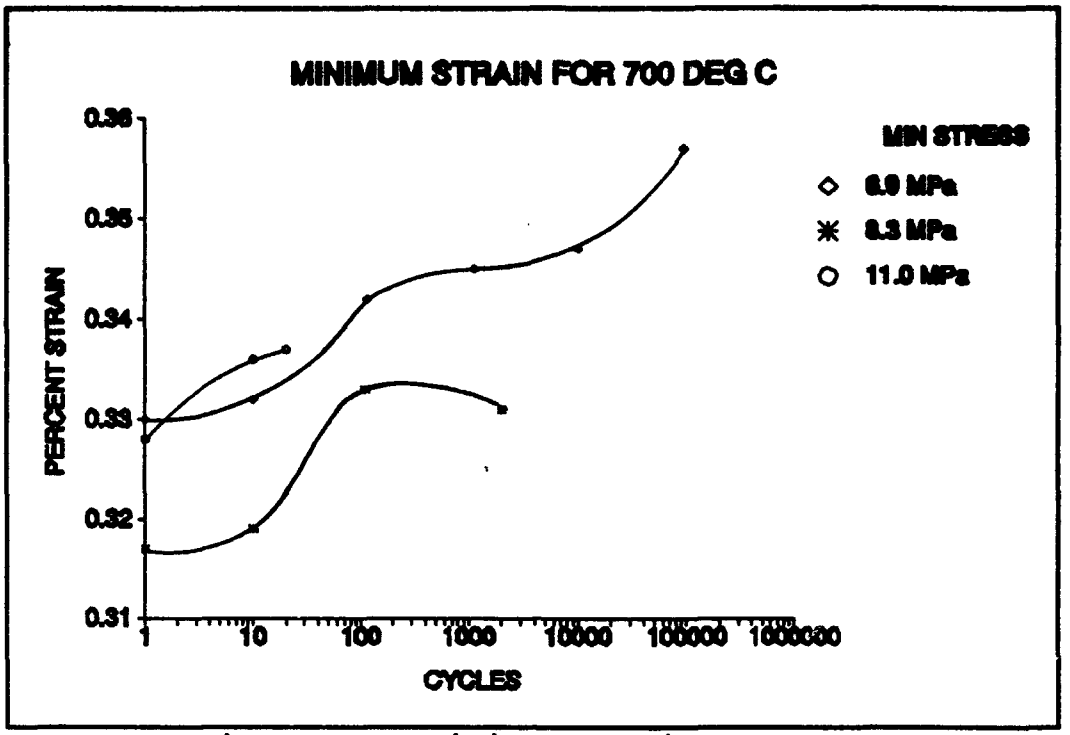

Figure 30. Minimum Strain, 700° C.

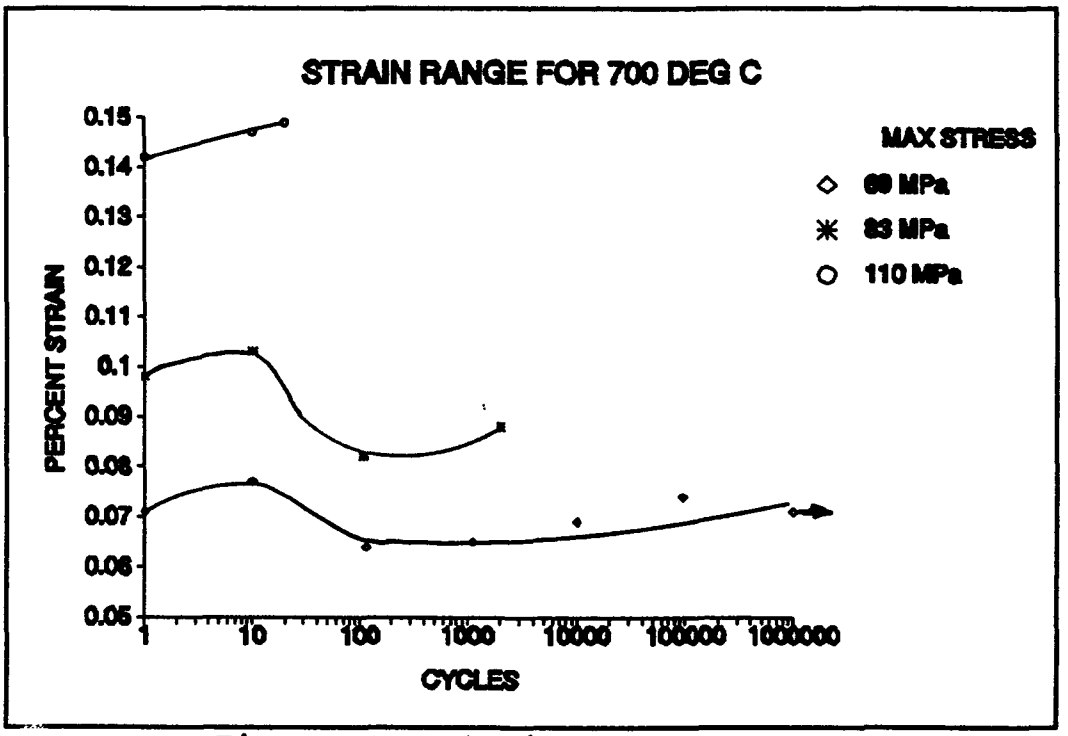

Figure 31. Strain Range, 700° C.

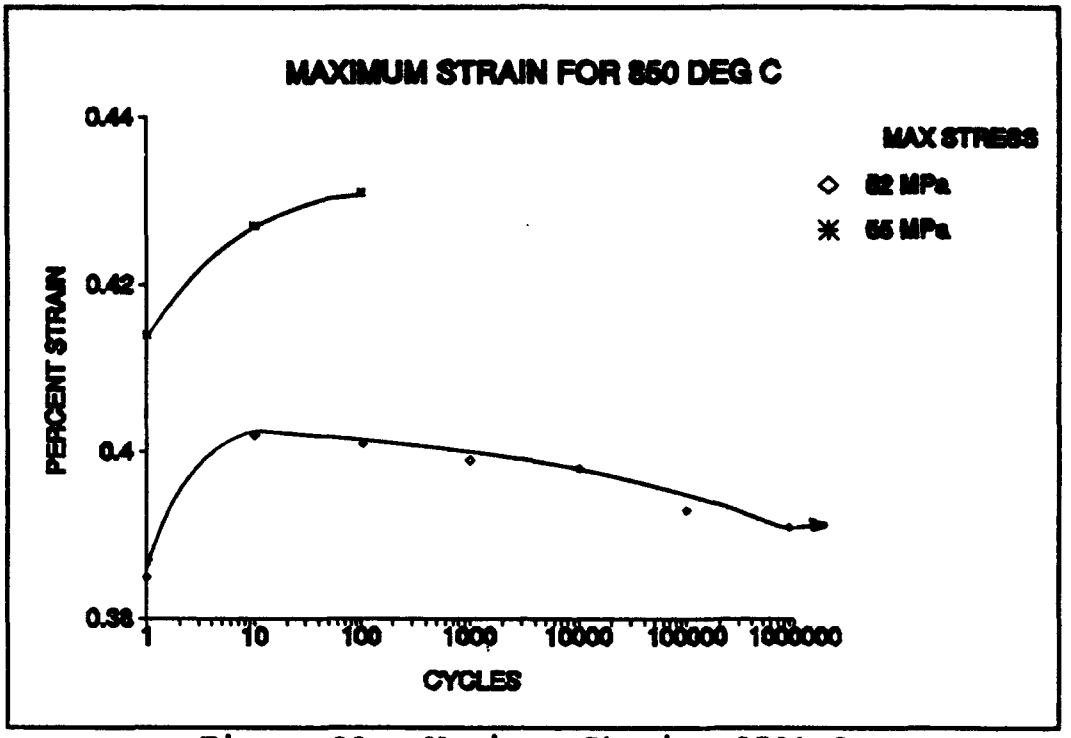

Figure 32. Maximum Strain, 850° C.

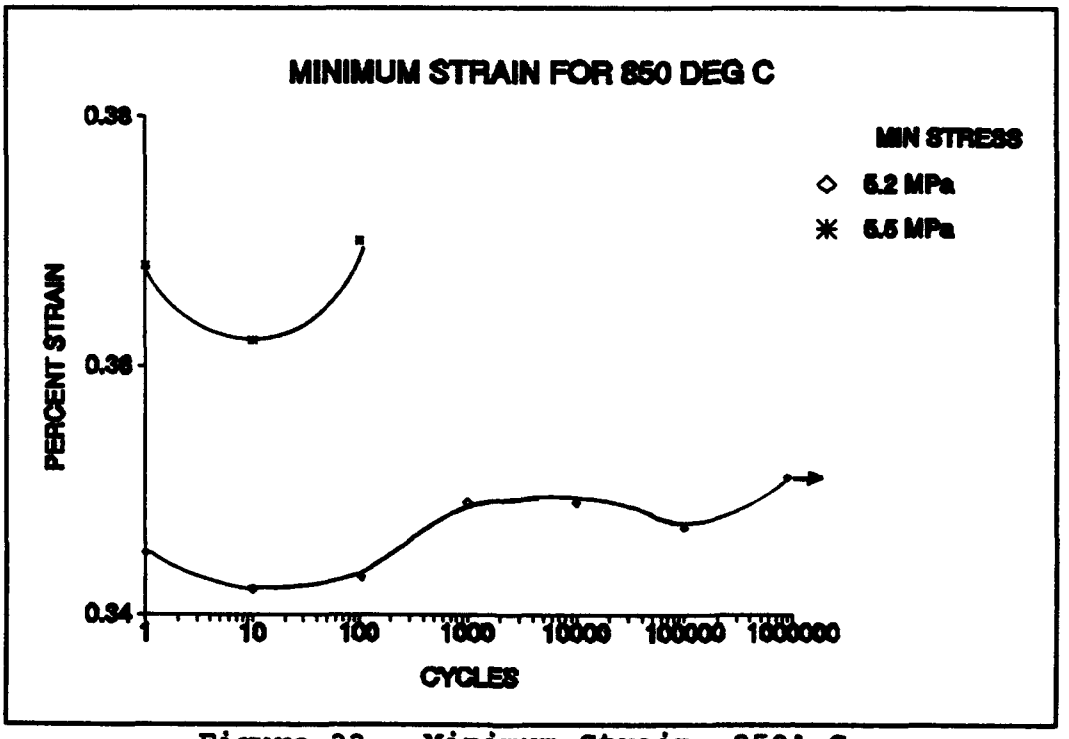

Figure 33. Minimum Strain, 850° C.

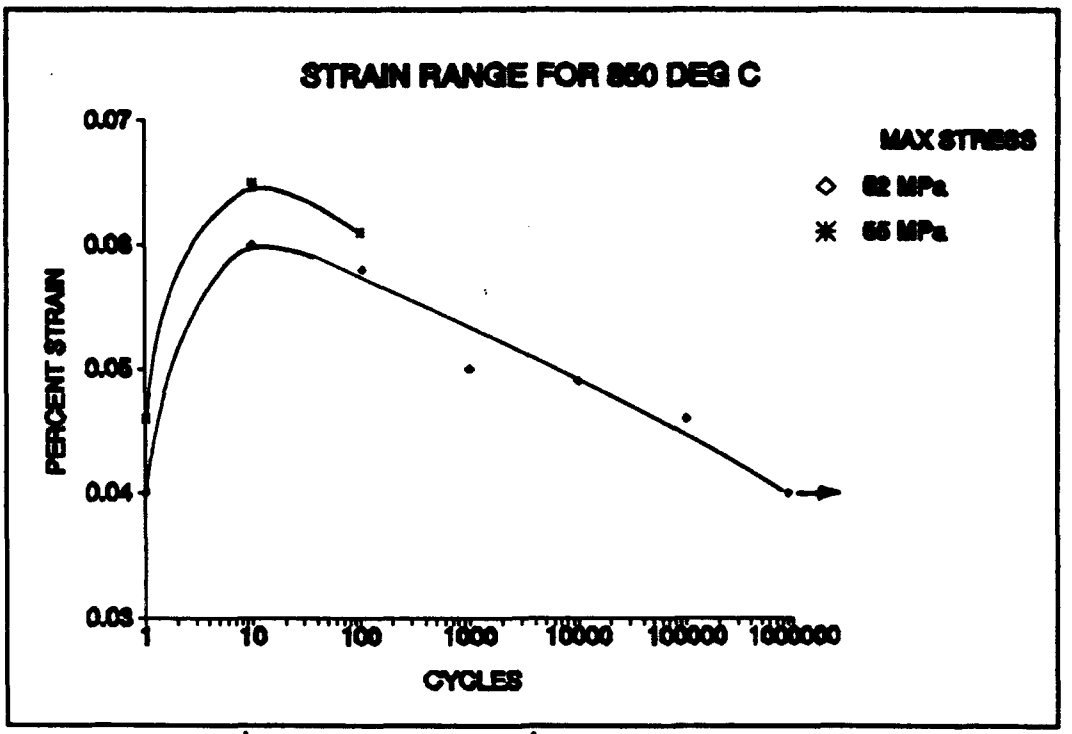

Figure 34. Strain Range, 850° C.

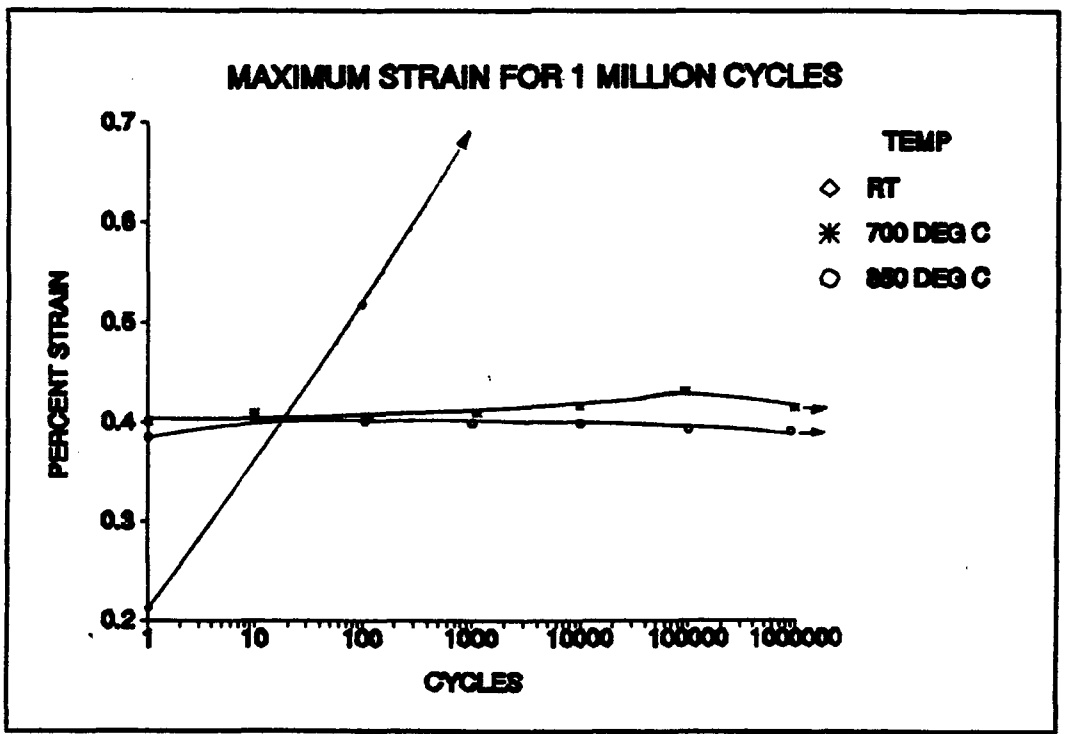

Figure 35. Maximum Strain for Runout Specimens.

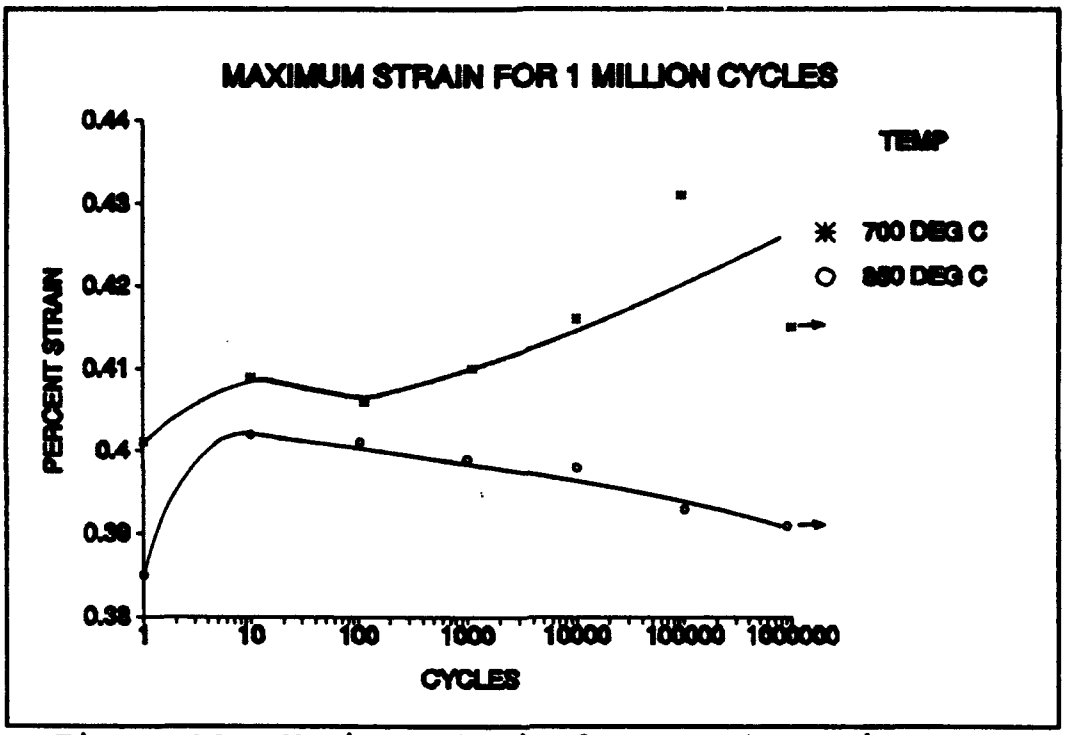

Figure 36. Maximum Strain for Runout Specimens at 700° and 850° C.

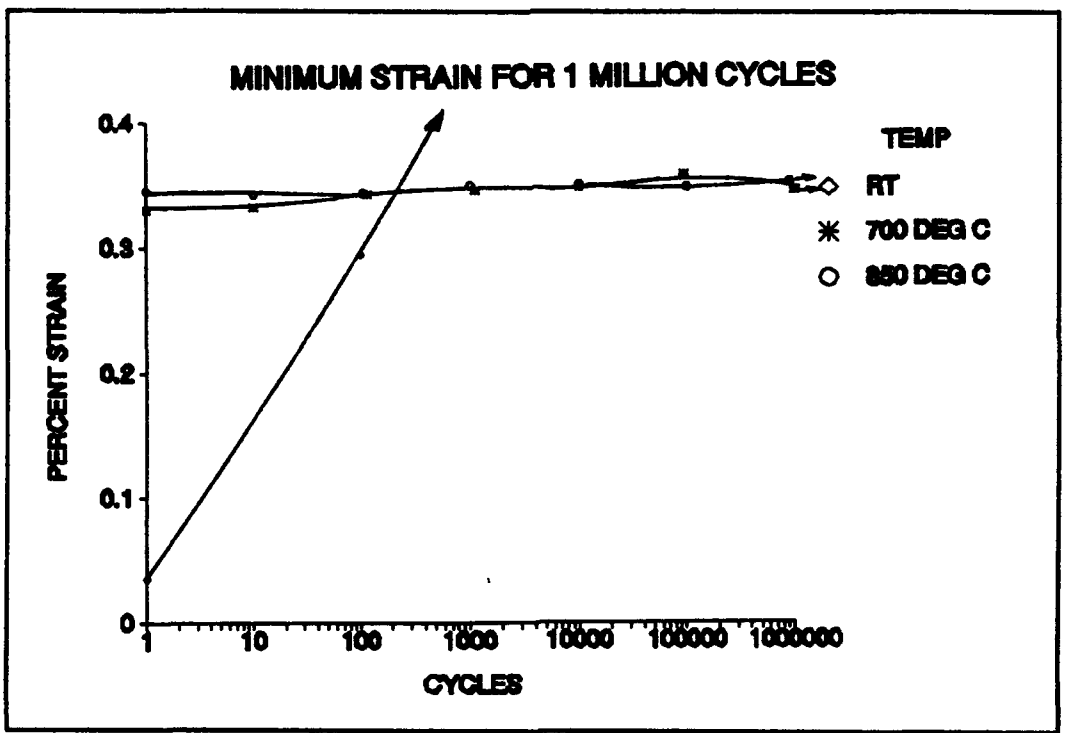

Figure 37. Minimum Strain for Runout Specimens.

less damage to the matrix, resulting in creating significantly less matrix debris.

Figure 38 shows the strain range for the specimens tested at three temperatures which reached cycle run out. The strain range for the specimens tested at RT and 700° C increased throughout the tests, which indicated that an accumulation of damage led to the final failure. However, at 850° C, the strain range initially increased for the first few cycles and then decreased, which indicated that different damage mechanisms were involved at this elevated temperature.

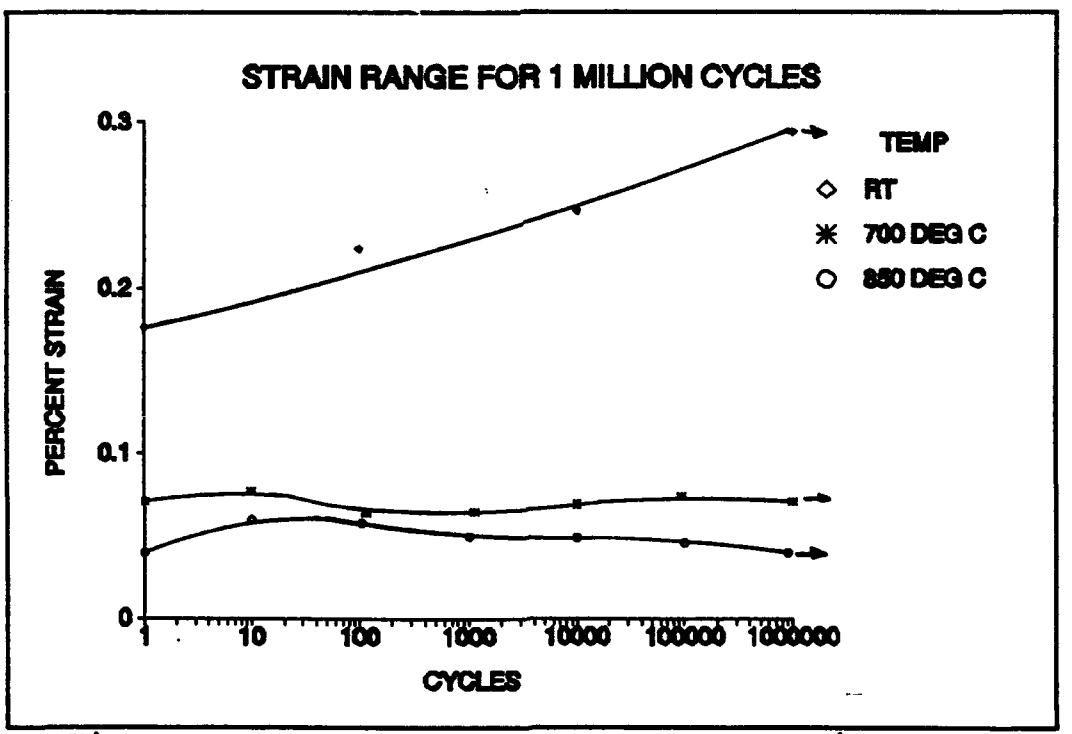

Figure 38. Strain Range for Runout Specimens.

D. Crack Density

Two interrupted tests were performed to obtain acetate edge replicas in order to investigate damage by studying crack density on the polished edge of a test specimen. One test was run at 700° C using a maximum stress of 73 MPa. Additionally, another interrupted test was run at 850° C with a maximum stress of 53 MPa. These loads, based on the results of the S-N curves in Section A, corresponded to an expected life of 100,000 cycles for both test specimens.

Unfortunately, very little data was gathered because the specimen tested at 700° C failed after only 7,671 cycles and the specimen tested at 850° C failed after only 380 cycles. Since these specimens failed much sooner than expected, the results of these tests were suspected to be influenced by thermo-mechanical fatigue and effects of increased periods of exposure to the elevated temperatures, both of which were beyond the scope of this particular study.

Figures 39 and 40 show the results of the crack growth analysis of the two interrupted tests that were performed. The specimen tested at 700° C developed many cracks in the 90° plies after the first cycle. The number of cracks in the 0° matrix was small after one cycle, but after 1,000 cycles, there were practically equal numbers of cracks in both the 0° and 90° plies. In the specimen tested at 850° C, however, notice that the number of cracks grew at

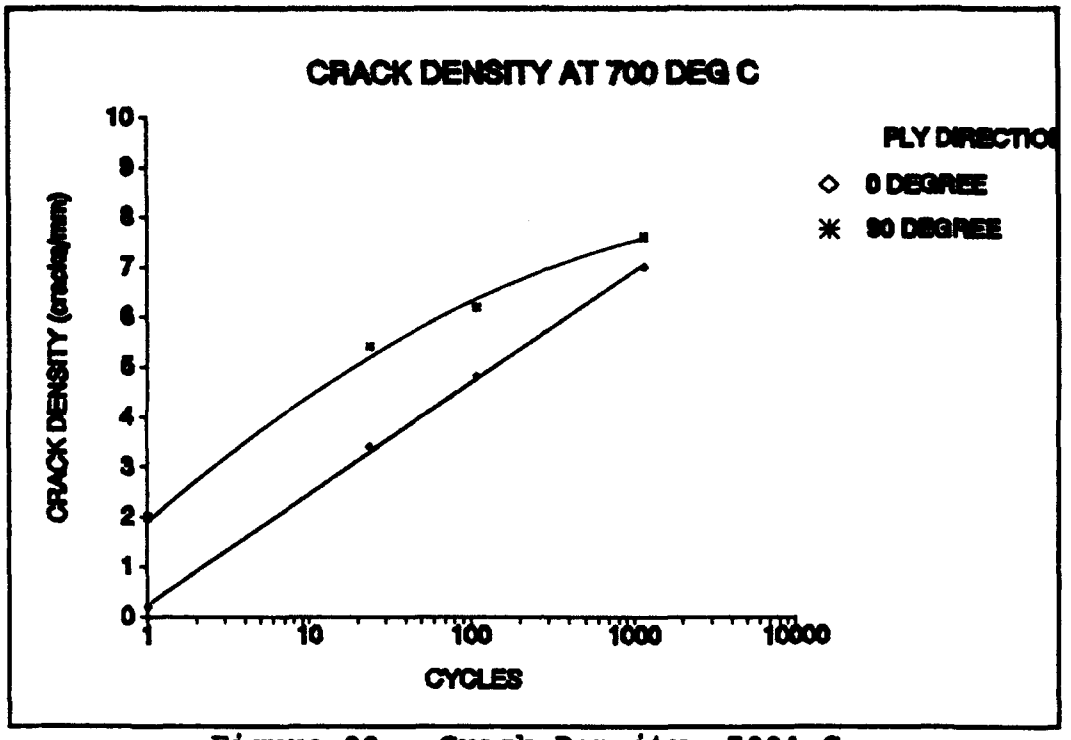

Figure 39. Crack Density, 700° C.

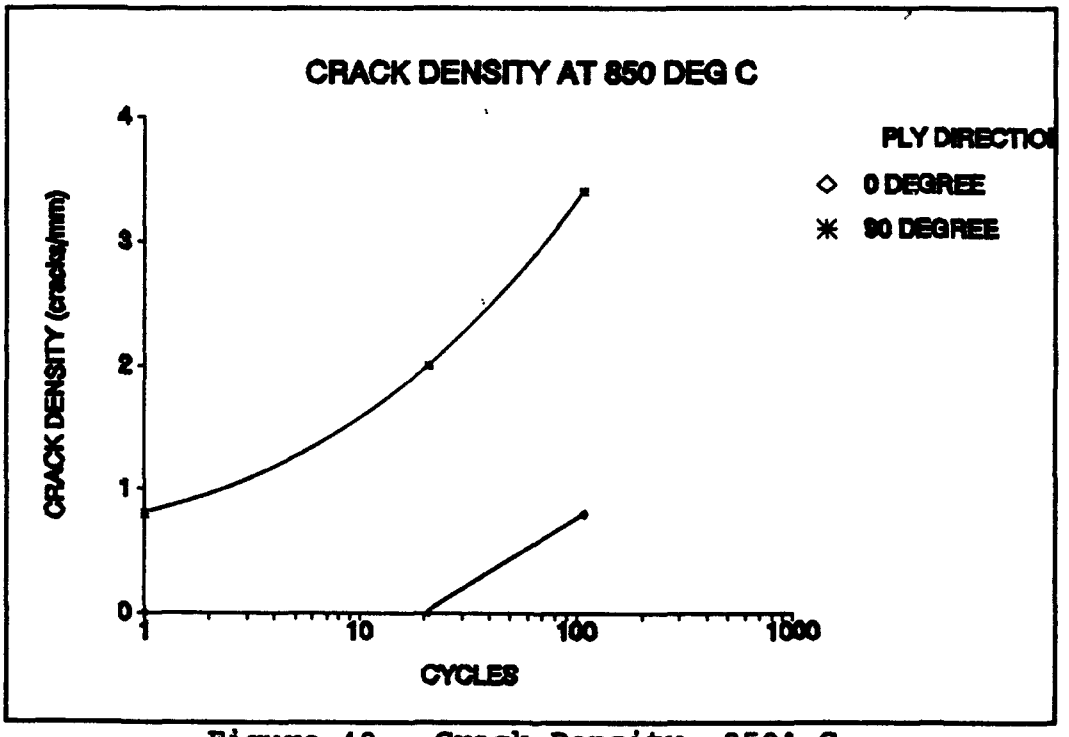

Figure 40. Crack Density, 850° C.

the same rates in both the 0° and 90° matrices. If the fibers were debonding from the matrix at 850° C, this decrease in the number of cracks would be as shown in Figure 40.

Figures 41 through 44 are photographs of acetate edge replicas that show the progression of crack growth during the 700° C interrupted test. Figure 41 shows the cracks first developed in the 90° plies. After 24 cycles, Figure 42 shows the cracks extending from the 90° plies into the 0° plies. Figures 43 and 44 show that the cracks gradually grew across the entire 0° plies before final failure occurred.

Figures 45 through 47 show the edge damage recorded in the specimen tested at 850° C. Significantly less damage occurred on the first cycle compared to the 700° C interrupted test. No pattern of damage accumulation in this series of edge replicas was evident. It was observed that the transverse cracks in the 90° plies did not grow into the 0° plies after 109 cycles as was clearly seen during the 700° C interrupted test. These findings, while incomplete, do support the damage mechanisms discussed in Sections A through D that ultimate failure in tension-tension fatigue loading at temperatures up to 700° C resulted from an accumulation of damage to the matrix.

Figure 41. Interrupted Test, 700° C, 1 Cycle, 50X.

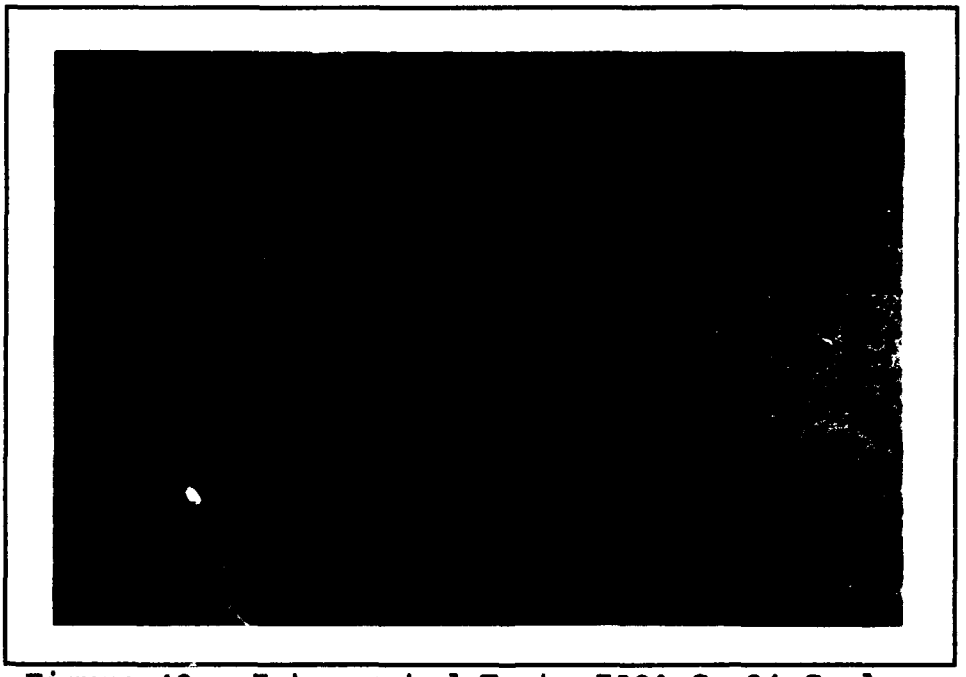

Figure 42. Interrupted Test, 700° C, 24 Cycles, 50X.

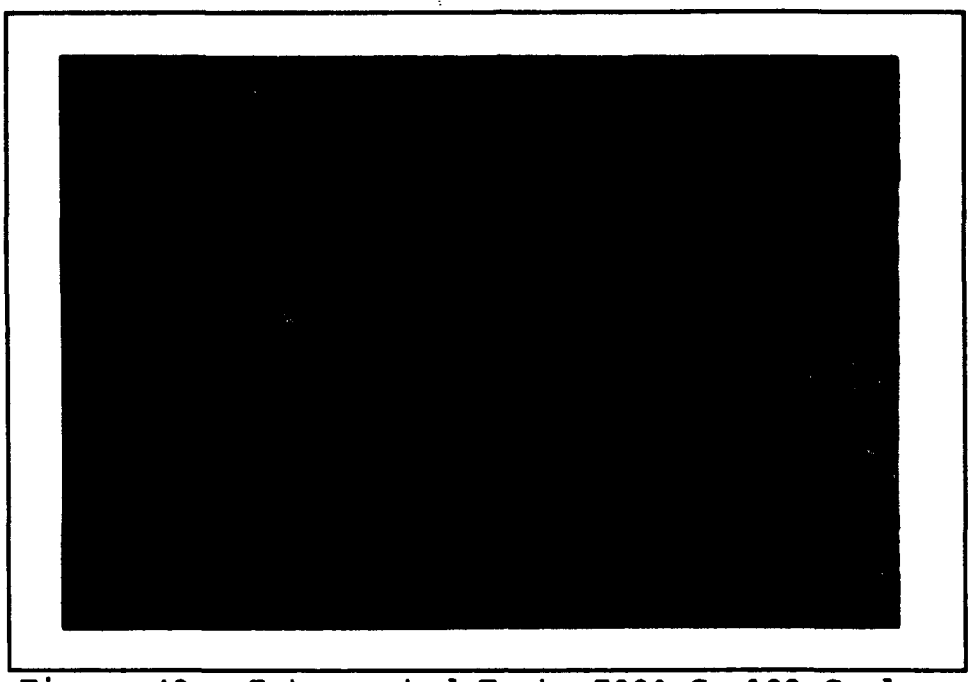

Figure 43. Interrupted Test, 700° C, 109 Cycles, 50X.

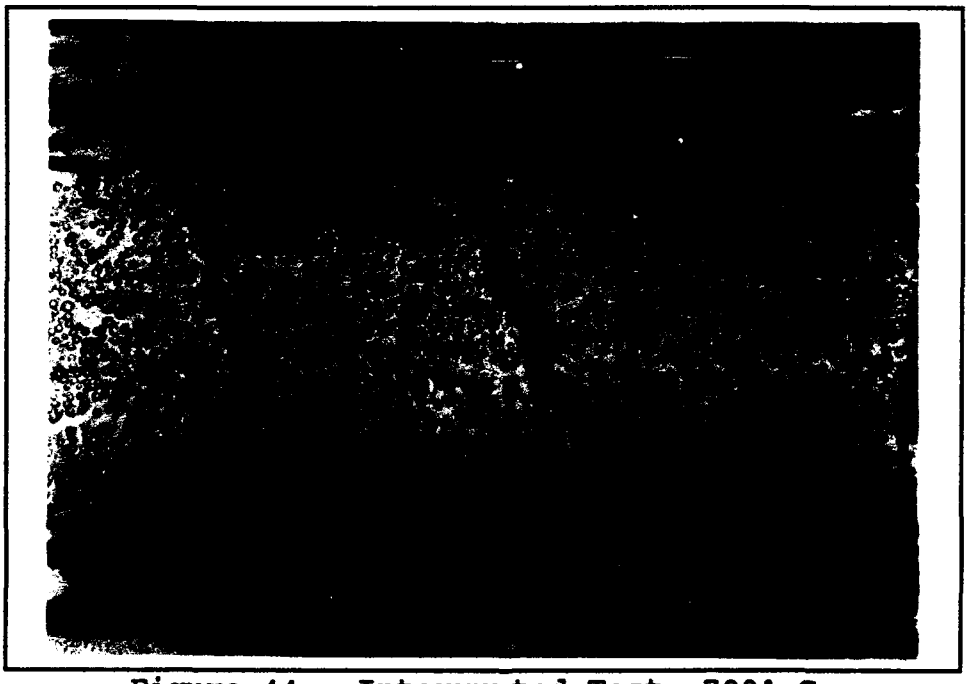

Figure 44. Interrupted Test, 700° C, 1,148 Cycles, 50X.

Figure 45. Interrupted Test, 850° C, 1 Cycle, 50X.

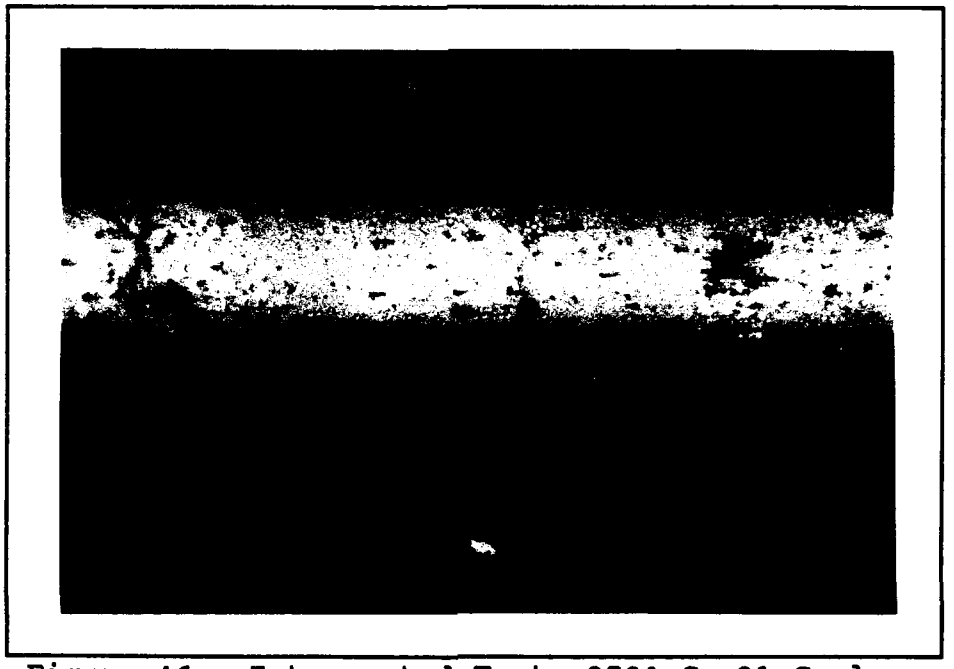

Figure 46. Interrupted Test, 850° C, 21 Cycles, 50X.

Figure 47. Interrupted Test, 850° C, 109 Cycles, 50X.

E. Hysterysis Loops

Another test parameter used to monitor damage progression is the area inside the hysterysis loop of the stress-strain curves. The area inside of these hysterysis loops was calculated using a computer program based on the trapezoid rule from calculus. This program is included in the Appendix. The units of this energy parameter were expressed in terms of energy, kJ/m^3.

This energy per unit volume term is useful when comparing specimens of different sizes. Therefore, the area of the hysterysis loops of the tests conducted for this

study at 700° C and 850° C were compared to the results of Opalski's study of fatigue tests conducted at RT [8].

At RT, the results of the energy versus cycles show that the largest energy value occurred during the first cycle of each test, as shown in Figure 48. This indicated that the most damage occurred during the first cycle, regardless of the number of cycles to which the specimen was subjected. For the specimen that failed, the energy slowly increased until failure occurred. For the other specimen which did not fail, the energy term remained constant after the first few cycles.

Figure 49 shows the energy versus cycles for the tests conducted at 700° C. The energy values show the same behavior as those for the RT tests. This indicated, once again, that the damage progression and damage mechanisms involved at RT and 700° C were very similar. However, at RT the energy did increase prior to final failure. At 700° C, this increase in energy was not observed.

Figure 50 shows that the trends observed at 850° C again differ significantly from those observed at RT and 700° C. Figure 50 shows that the minimum energy occurred during the first cycle. This can be explained by recalling from Section D of this chapter that at 850° C, fewer cracks appeared in the matrix during the first few cycles when compared to the test run at 700° C, which caused less maximum strain.

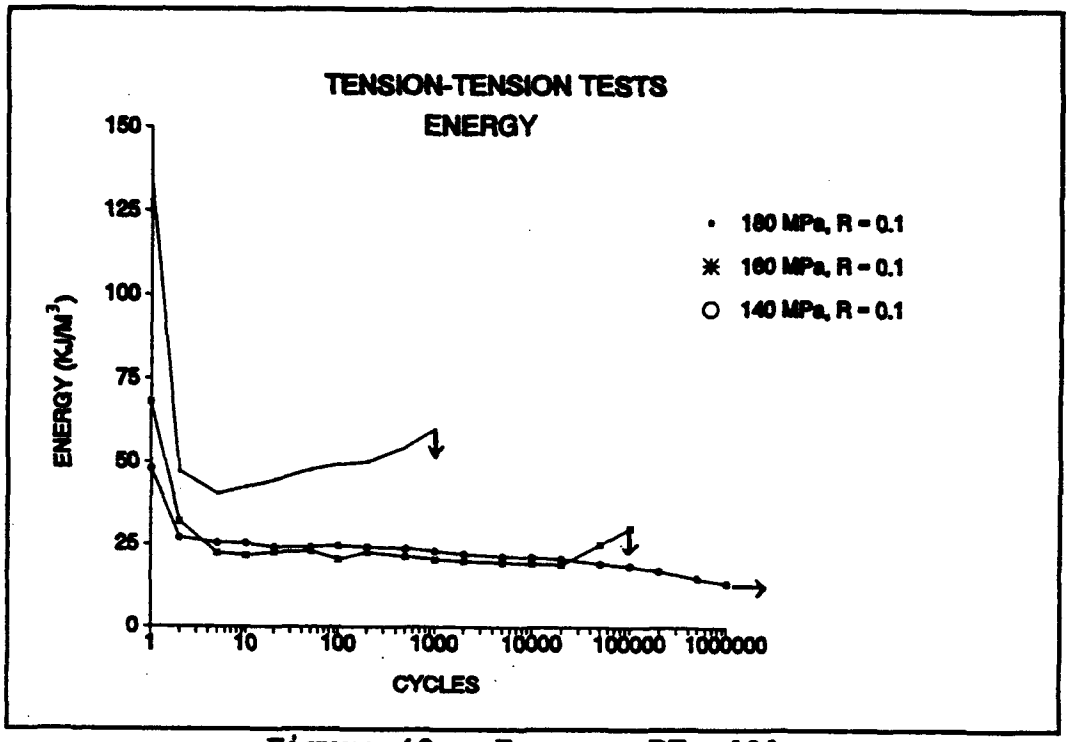

Figure 48. Energy, RT, [8].

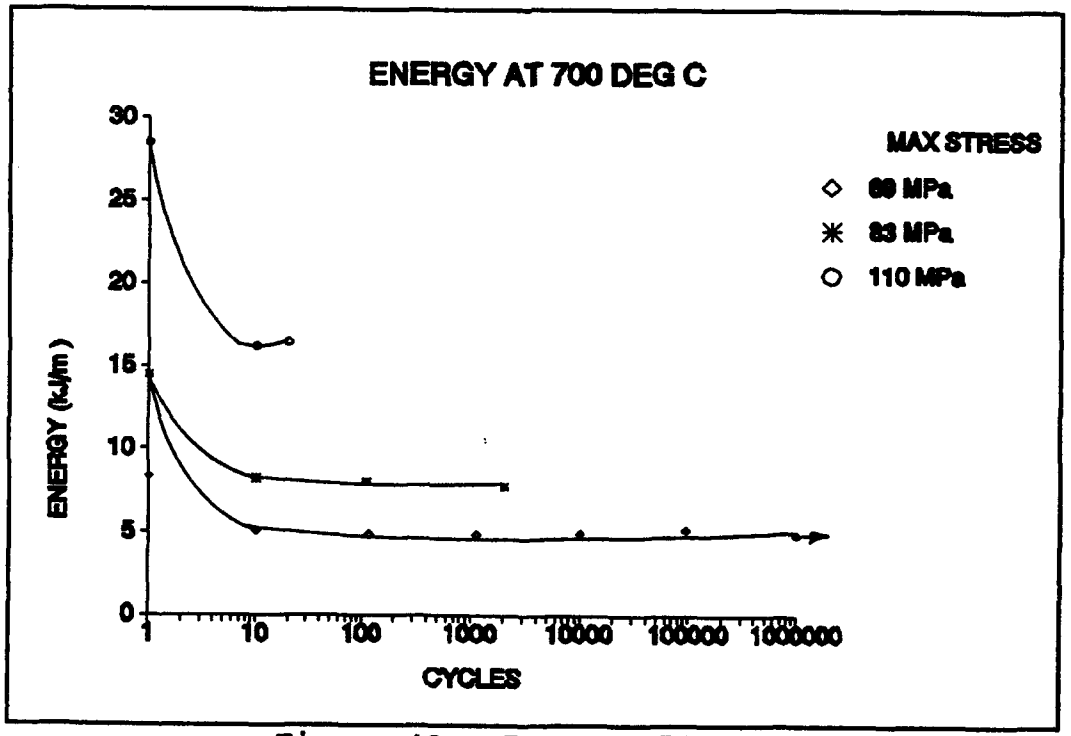

Figure 49. Energy, 700° C.

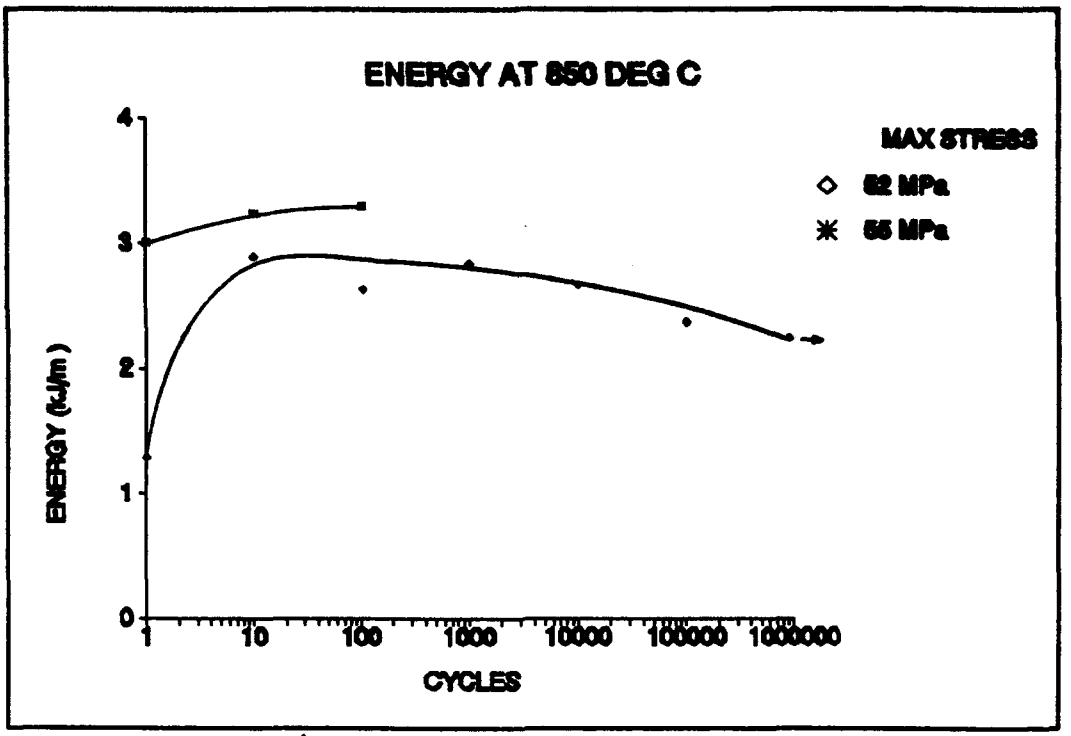

Figure 50. Energy, 850° C.

At 850° C, the fibers began to debond from the matrix after the first few cycles, which caused the energy term to increase during these tests. As the number of debonded fibers increased, the energy continued to increase as shown in Figure 50. Then, as the test which reached cycle run out continued, the debonded fibers oxidized and stiffened, and the energy decreased due to no further damage after approximately 10,000 cycles.

F. Fractography

Three specimens were sectioned and lightly polished to show evidence that fibers had debonded during the 850° C tests. From these specimens, a thin wafer was removed by

making two cuts perpendicular to the loading axis, approximate 3 mm apart. These wafers were then mounted and lightly polished. This enabled viewing of the 0° fibers, parallel to the loading axis.

Figure 51 shows the cross-section of a specimen perpendicular to the loading axis. It clearly shows that the overall damage occurred near the edge of a specimen, which was tested at 850° C for 1 million cycles. The 0° plies were inspected near the large cracks and several debonded fibers were found. Figures 52 and 53 clearly show several fibers of the 0° plies that debonded after the cracks in the matrix exposed them to the 850° C environment.

Specimen 2, which was tested at 700° C for 1 million cycles, was also sectioned for inspection and compared to the 850° C specimens. Figure 54 shows that large cracks developed in the matrix of the specimen. The specimen was investigated near these large cracks and no evidence of debonded fibers was observed. Figure 55 shows that as the crack progressed through the 0° matrix, exposure to the 700° C environment caused no fiber debonding. Although the crack took advantage of the weak interface between the fiber and matrix to go around the fibers, environmental debonding was not observed as in specimen shown in Figures 52 and 53.

Figure 56 shows a cross-section removed from a point of specimen 10 that was not exposed to the high temperature

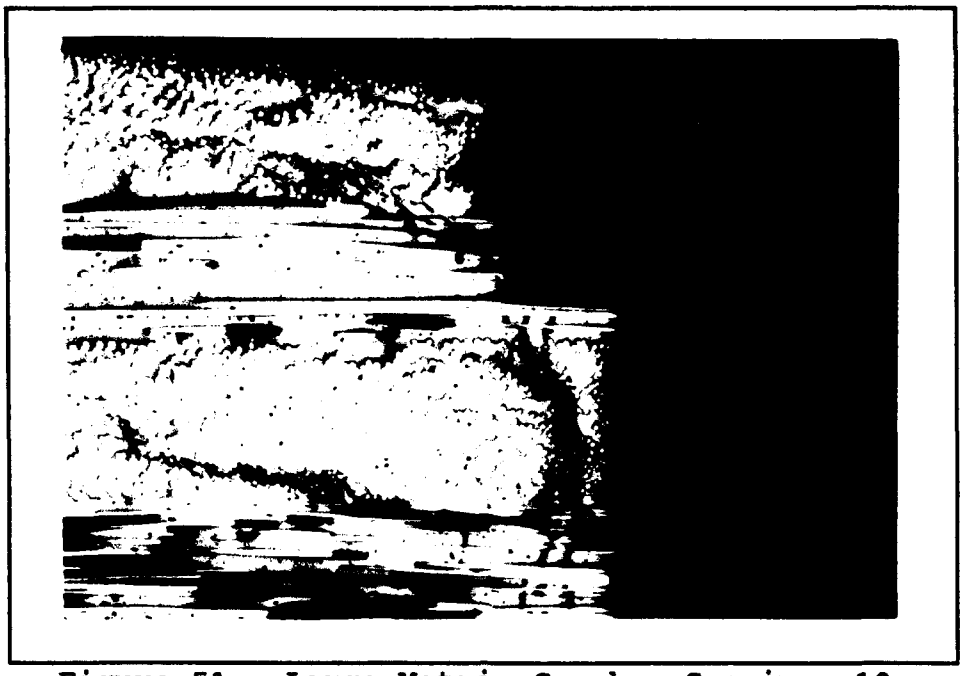

Figure 51. Large Matrix Cracks, Specimen 10, (Load Perpendicular to Page), 50X.

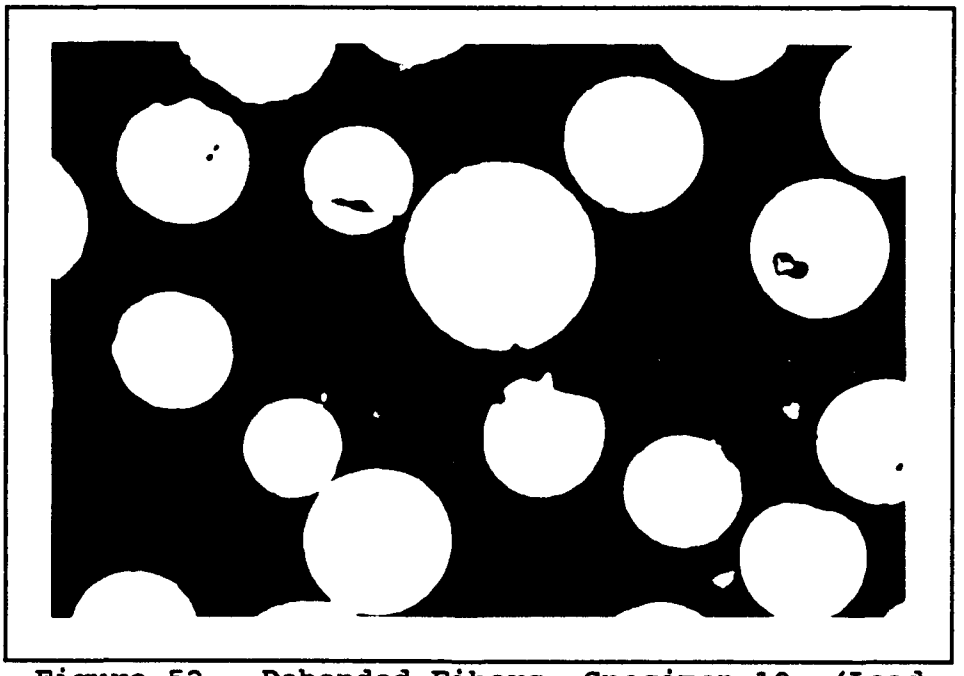

Figure 52. Debonded Fibers, Specimen 10, (Load Perpendicular to Page), 1000X.

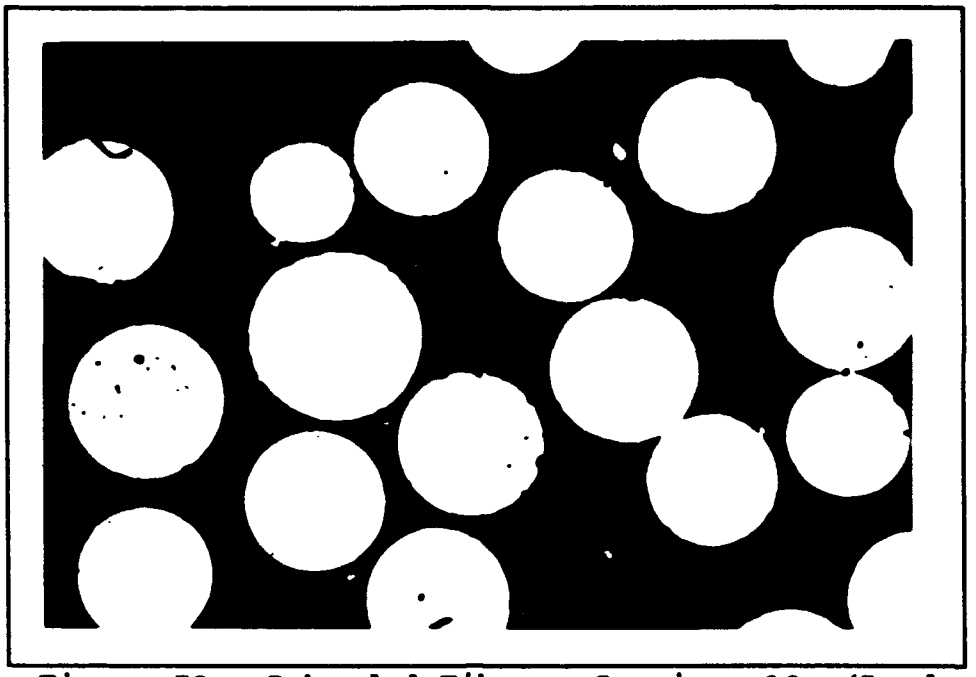

Figure 53. Debonded Fibers, Specimen 10, (Load Perpendicular to Page), 1000X.

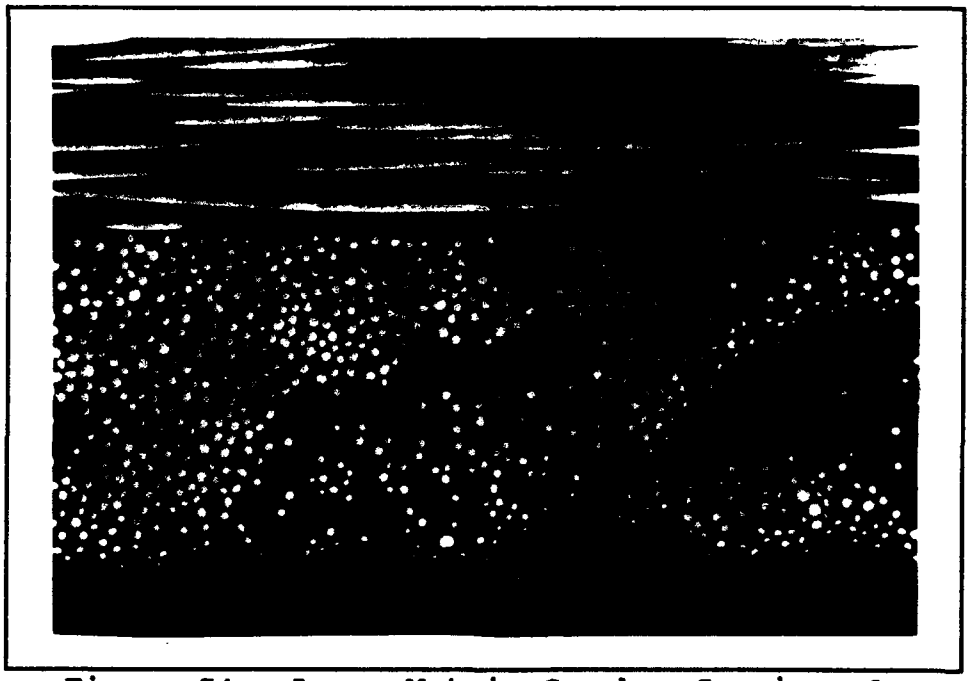

Figure 54. Large Matrix Cracks, Specimen 2, (Load perpendicular to Page), 50X.

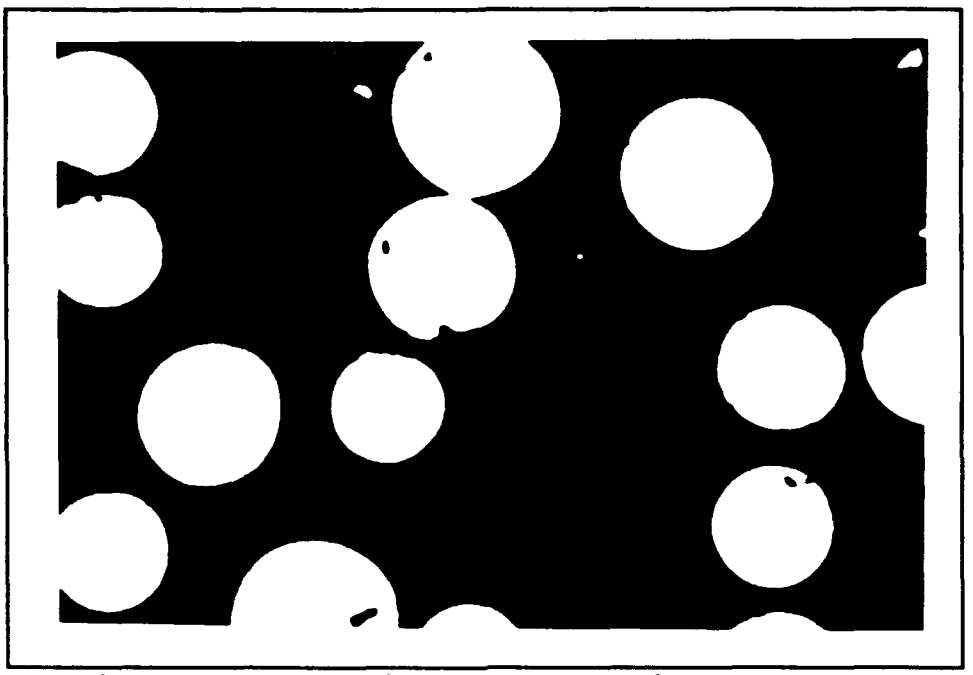

Figure 55. Matrix Crack, Specimen 2, (Load Perpendicular to Page), 1000X.

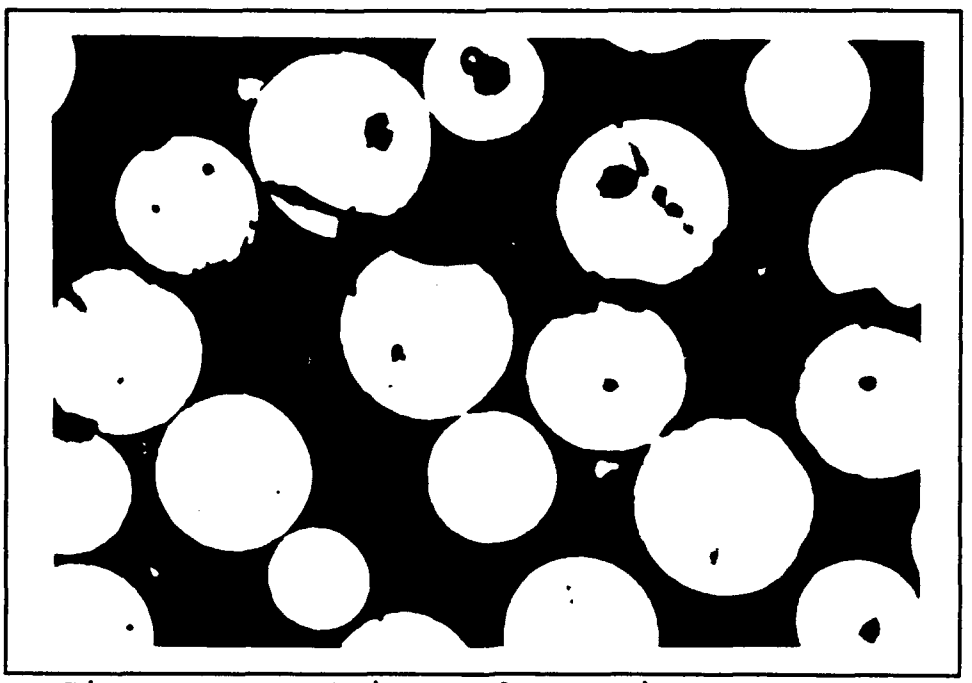

Figure 56. Matrix Crack, Specimen 10, (Load Perpendicular to Page), 1000X.

environment. This cross-sectioned wafer was used as a control section to compare the damage of specimen 10 at approximately RT versus 850° C. It was observed that the part of specimen 10 that was at RT during the fatigue test did sustain damage, but not in the form of debonded fibers.

Finally, the fracture surface of the failed specimens were investigated using the scanning electron microscope. Figures 57 through 60 show the fracture surfaces and fracture profiles of the specimens that failed during RT testing. The fracture surfaces were very rough and uneven, which indicated extensive damage occurred to the matrix prior to ultimate failure. The fracture profiles of these specimens were very jagged, which indicated that the final failure was due to small cracks that grew together and formed the large crack that caused ultimate failure. Extensive matrix damage was noticed along the edge near the final fracture.

Figures 61 through 64 show the fracture surfaces and fracture profiles of the specimens tested at 700° C that failed before reaching cycle run out. As in the case of failure surfaces of the specimens tested at RT, rough and uneven fracture surfaces were observed for these specimens tested at 700° C. The fracture profiles were also jagged for these specimens, which indicated that the final fracture surface was formed by cracks in the transverse plies that grew together as cracks developed through the 0°

Figure 57. Fracture Surface, Specimen 10*, RT, 7X.

Figure 58. Fracture Profile, Specimen 10*, RT, 12X.

Figure 59. Fracture Surface, Specimen 7*, RT, 9X.

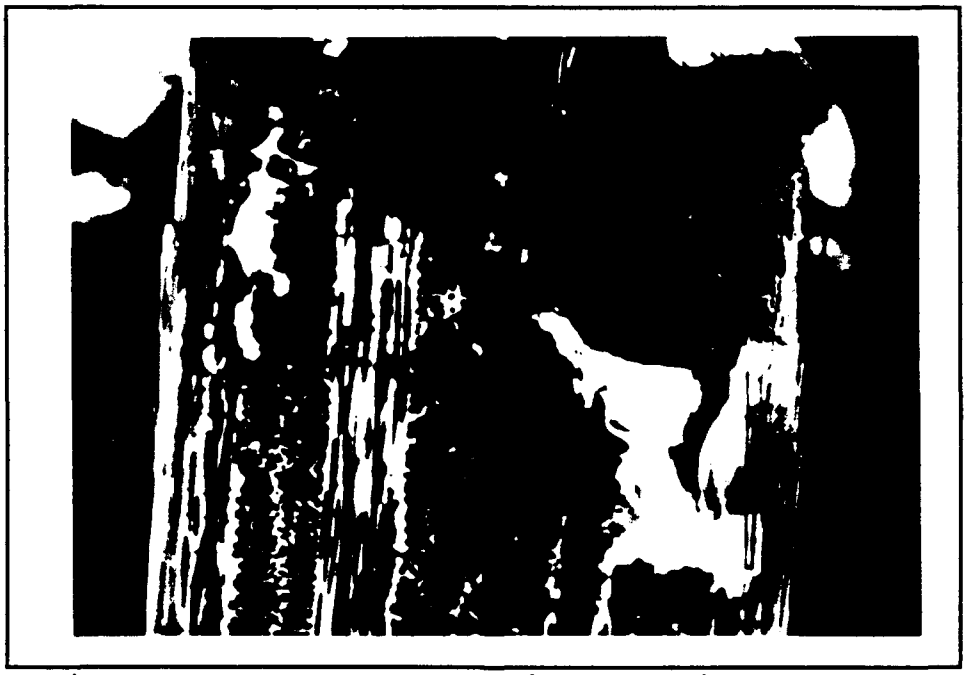

Figure 60. Fracture Profile, Specimen 7*, RT, 18X.

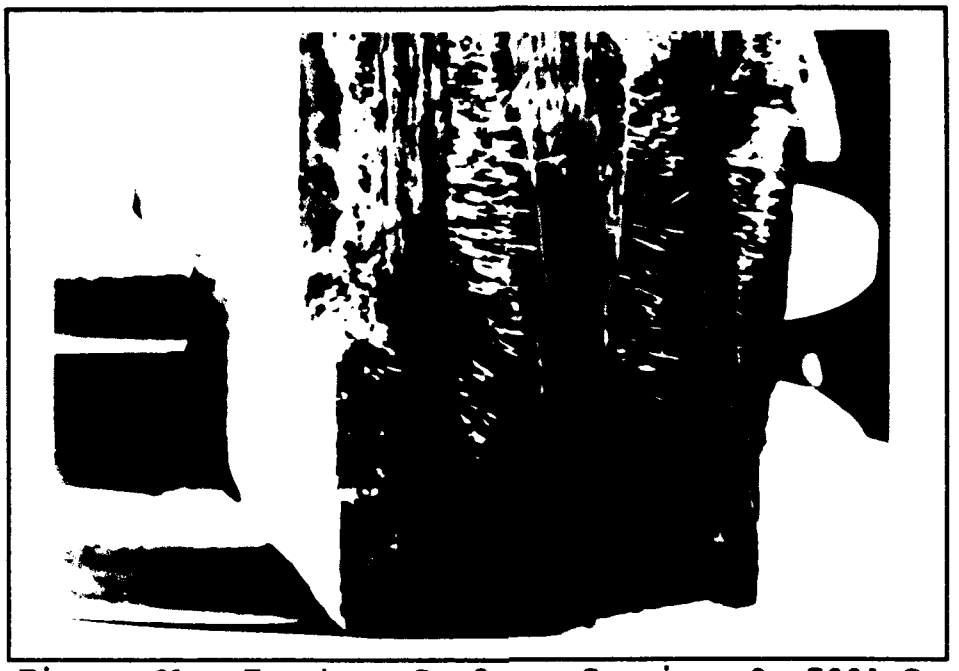

Figure 61. Fracture Surface, Specimen 3, 700° C, 15X.

Figure 62. Fracture Profile, Specimen 3, 700° C, 22X.

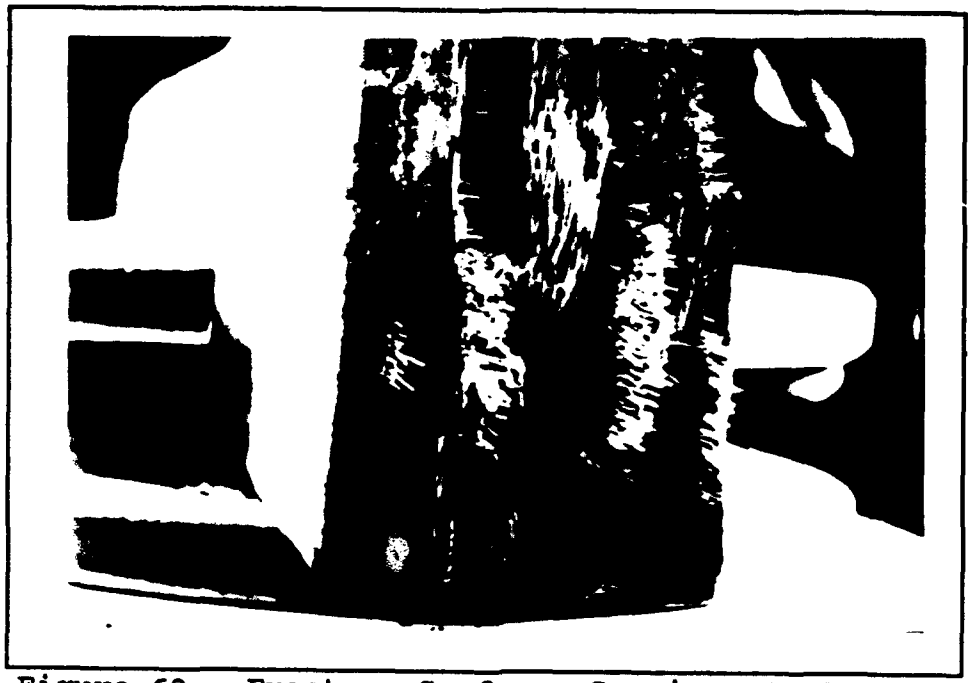

Figure 63. Fracture Surface, Specimen 4, 700° C, 14X.

Figure 64. Fracture Profile, Specimen 4, 700° C, 23X.

plies. Figure 62 clearly shows both transverse and longitudinal cracks, which are also seen in the RT tested specimen shown in Figure 58. This evidence further supports that the damage mechanisms were identical at both RT and 700° C.

However, the fracture surface and fracture profile of the specimen tested at 850° C were observed to be quite different from those of the specimens tested at the lower temperatures. Figure 65 shows a flat, smooth fracture surface similar to the one observed by Butkus and others in their tests at temperatures above 800° C [10]. It can be observed in Figure 65 that the crack initiated in the top right corner of the specimen and grew through the specimen until final failure occurred. It can be also observed in Figure 66 that the edge of the specimen showed no damage to the matrix other than the final fracture, which was different than the one observed in the RT and 700° C fracture profiles. Also, in Figure 66, it can be observed that several long fibers protruded from the fracture surface. These long fibers supported the previous observations of debonded fibers at 850° C.

Figure 65. Fracture Surface, Specimen 5, 850° C, 13X.

Figure 66. Fracture Profile, Specimen 5, 850° C, 22X.

V. Conclusions

In summary, the purpose of this study was to investigate the damage mechanisms involved in a Nicalon/CAS cross-ply ceramic matrix composite material when subjected to tension-tension fatigue loading at elevated temperatures. Static tests and tension-tension fatigue tests at both 700° C and 850° C were performed. The results of these tests were compared to existing data from research studies previously done at room temperature (RT) and 815° C.

The results of the tests performed at 700° C showed the same damage behavior as the results of tests previously performed at RT. The static test results, fatigue life results, and normalized modulus results showed that the ultimate strength of the composite was reduced at 700° C when compared to that at RT. However, the general damage behavior and damage mechanisms involved were the same up to 700° C.

Furthermore, it was noticed from microscopic examination of specimen cross-sections that as the temperature was increased to 700° C, the strength of the bond between the fibers and the matrix was noticeably weakened. However, even though this bond was weakened, it did not significantly affect the overall behavior of the material, or change the damage mechanisms from those seen for the RT tests.

At 850° C, however, fiber debonding significantly changed the tension-tension fatigue response of the cross-ply material. The fibers began to debond after only a few cycles, and the longitudinal fibers supported the entire load. The fatigue life curve for 1 million cycles showed this by having a flat response after only 300 cycles. The normalized modulus, strain, and area in the stress-strain hysterysis loops all showed that the longitudinal fibers had large scale debonding within the first 10 cycles and supported the entire load soon after.

Investigation of the crack density showed that the matrix material sustained less damage at 850 ° C than at 700° C. This further supported the theory of rapid fiber debonding at a temperature of 850° C.

Fractographic evaluation also showed that the material tested at 850° C had many fibers debonded. Examination of a test specimen that lasted only 360 cycles showed debonded fibers, which proved that it occurred very rapidly after being exposed to the high temperature environment.

VI. Recommendations

The tension-tension fatigue behavior of the Nicalon/CAS cross-ply ceramic matrix composite is now well known at elevated temperatures. With fiber debonding as the main damage mechanism in the high temperature environment, further studies are necessary that concentrate on what causes the fibers to come in contact with the environment.

The primary applications of interest for ceramic composites involve high temperatures. Therefore, it would seem appropriate that the effects of creep and thermo-mechanical fatigue should next be investigated for this material.

Bibliography

1. Zawada, L.P., Butkus, L.M., and Hartman, G.A., "Tensile and Fatigue Behavior of Silicon Carbide Fiber-Reinforced Aluminosilicate Glass," Journal of the American Ceramic Society, Vol 74, No 11, November 1991, pp 2851-2858

2. Dauskardt, R.H., Ritchie, R.O., and Cox, B.N., "Fatigue of Advanced Materials: Part II," Advanced Materials and Processes, Vol 144, No 2, August 1993, pp 30-35

3. Sorensen,B.F., Talreja, R., and Sorensen, O.T., "Damage Development in a Ceramic Matrix Composite under Mechanical Loading," Proceedings of the 5th European Conference on Composite Materials, Bordeaux, France, April 1992, pp 613-618

4. Daniel, I.M., Anastassopoulos, G., and Lee, J.W., "Failure Mechanisms in Ceramic Matrix Composites," 1989 SEM Spring Conference on Experimental Mechanics, Cambridge, MA, May 1989, pp 832-838.

5. Karandikar, P.G., and Chou, T.W., "Microcrack Growth and Moduli Reductions in Nicalon-CAS Composites under Static Fatigue and Cyclic Fatigue," Proceedings of the American Society for Composites Seventh Technical Conference, Technomic Publishing Co, Lancaster, PA, 1992

6. Karandikar, P., and Chou, T.W., "Characterization and Modelling of Microcracking and Elastic Moduli Changes in Nicalon/CAS Composites," Composites Science and Technology, Vol 46, No 2, 1993

7. Kuo, W.S., and Chou, T.W., "Nonlinear and Damage Behavior of Ceramic-Matrix Cross-Ply Composites," Proceedings of the Ninth International Conference on Composite Materials, Vol 2, 1993, pp 47-54.

8. Opalski, F.A., Fatigue Behavior of a Cross-Ply Ceramic Matrix Composite Under Tension-Tension and Tension-Compression Loading, MS Thesis, AFIT/GAE/ENY/92D-02,School of Engineering, Air Force Institute of Technology (AU), Wright-Patterson AFB, Ohio, December 1992

9. Zawada, L.P., Pernot, J.J., and Butkus, L.M., "Fatigue Behavior of Several Ceramic Matrix Composites," Proceedings of the Fifth International Conference on Fatigue and Fatigue Thresholds, Vol 3, Montreal, Canada, 1993, pp 1307-1312.

10. Butkus, L.M., Zawada, L.P., and Hartman, G.A., "Fatigue Test Methodology and Results for Ceramic Matrix Composites at Room and Elevated Temperatures," Cyclic Deformation, Fracture, and Nondestructive Evaluation of Advanced Materials, ASTM STP 1157, M.R. Mitchell and O. Buck, Eds., American Society for Testing and Materials, Philadelphia, 1992, pp. 52-68.

11. Rousseau, C.Q., "Monotonic and Cyclic Behavior of a Silicon Carbide/Calcium-Aluminosilicate Ceramic Composite," Thermal and Mechanical Behavior of Metal Matrix and Ceramic Matrix Composites, ASTM STP 1080, Editors, Kennedy, J.M., Moeller, H.H., and Johnson, W.S., American Society for Testing and Materials, Philadelphia, 1990, pp 136-151

12. Stewart, R.L., and others, "Fracture of Si/C Fiber/Glass-Ceramic Composites as a Function of Temperature," Fracture Mechanics of Ceramics, Vol 7, Plenum Press, New York, 1986.

13. Holmes, J.W., Fatigue of Fiber Reinforced Ceramics, To Be Published.

14. Agins, D. ., Static Fracture Behavior af a Ceramic Matrix Composite at Elevated Temperatures, MS Thesis, AFIT/GAE/ENY/93D-1, School of Engineering, Air Force Institute of Technology (AU), Wright-Patterson AFB, Ohio, December 1993

15. Agarwal, B.D., and Broutman, L.J., Analysis and Performance of Fiber Composites, 2nd Ed., John Wiley and Sons, New York, 1990

Appendix

Energy Calculation Program

```
REM ENERGY.BAS, WRITTEN IN QBASIC
REM This program uses the trapezoidal rule to estimate the
REM area inside the hysterysis loop of a data acquisition REM
cycle obtained using MATE high cycle fatigue software.
REM Written by:  Captain Rick Tuznik
REM              AFIT/ENY
REM              WPAFB Ohio
REM Last Revised:  23 Aug 93

REM Definition of Variables:
REM KIPS     Instantaneous load (column #1 of data file)
REM STRESS   Instantaneous stress
REM STRAIN   Instantaneous strain
REM AREA     Specimen cross-sectional area
REM GAGE     Specimen gage length
REM SUM      Area inside hysterysis loop
REM BOX      Area below line connecting last data point to
               first data point

REM Dimension variable arrays

DIM STRESS(1000), STRAIN(1000), KIPS(1000), DISP(1000)

REM Set initial values of variables

SUM = 0
INPUT "ENTER AREA"; AREA
INPUT "ENTER GAGE LENGTH"; GAGE

REM Open and input MATE data file

INPUT "ENTER FILENAME"; N$
OPEN N$ FOR INPUT AS #1

REM Convert load(kips) and displacement(in) to stress(MPa)
REM and strain(mm/mm)

J = 1
DO
INPUT #1, KIPS(J), DISP(J)
STRAIN(J) = DISP(J) / GAGE
STRESS(J) = ((DIPS(J) * 1000 / AREA) * 6895)
J = J + 1
LOOP UNTIL (EOF(1))
```

```
REM Calculate area of hysterysis loop using trapezoidal
REM rule

FOR I = 2 TO 1000
N = I - 1
SUM = (SUM+((STRESS(I)+STRESS(N))/2*(STRAIN(I)-STRAIN(N))))
NEXT I

REM Subtract area below line connecting last and first data
REM points

BOX = (STRESS(1000)+STRESS(1))/2*(STRAIN(1000)-STRAIN(1))
SUM = SUM - BOX

REM Print solution to screen

PRINT "THE ENERGY(J/m³) = "; SUM

REM Close input file

CLOSE
END
```

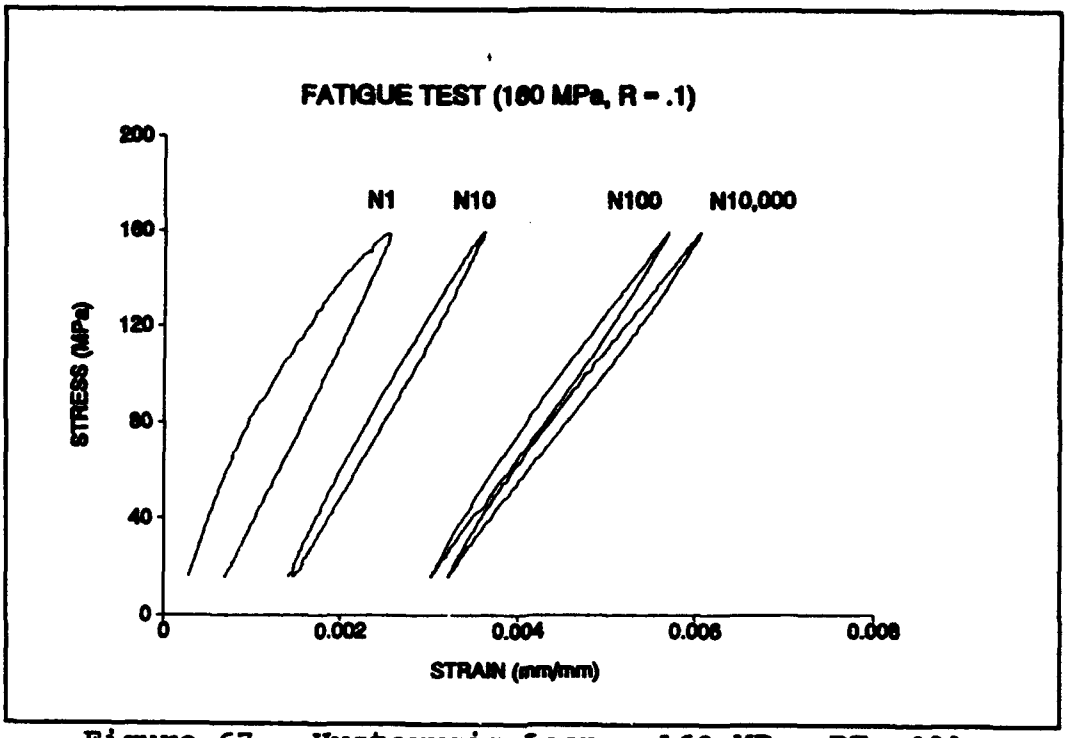

Figure 67. Hysterysis Loops, 160 MPa, RT, [8].

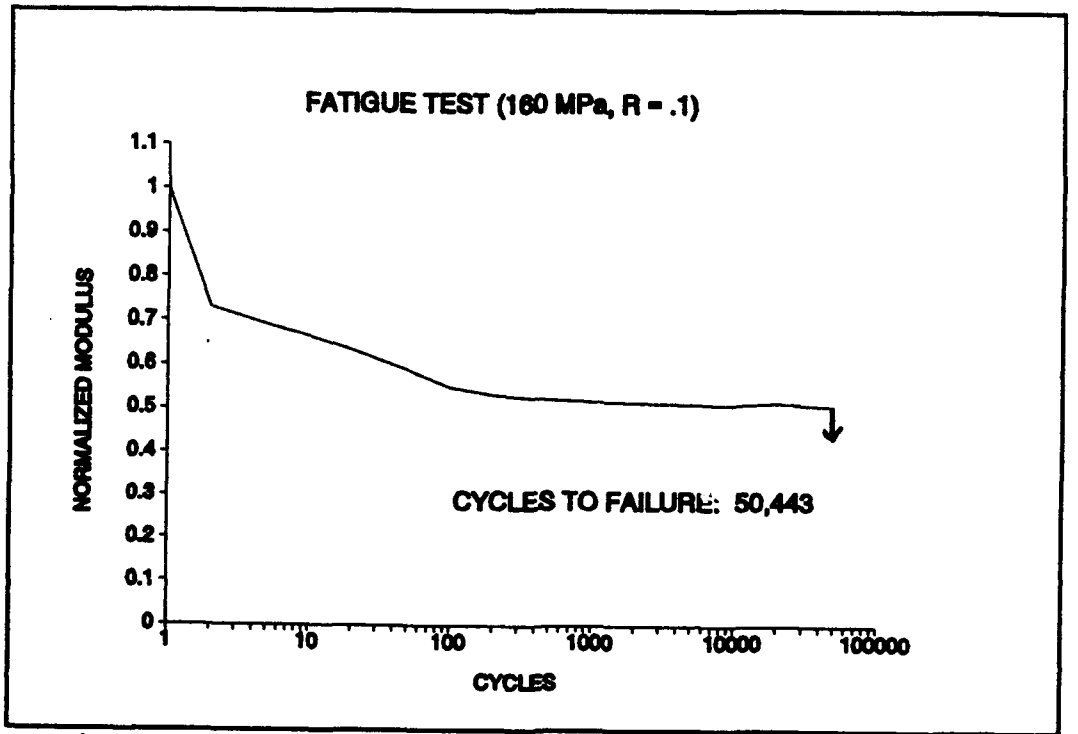

Figure 68. Modulus Degradation, 160 MPa, RT, [8].

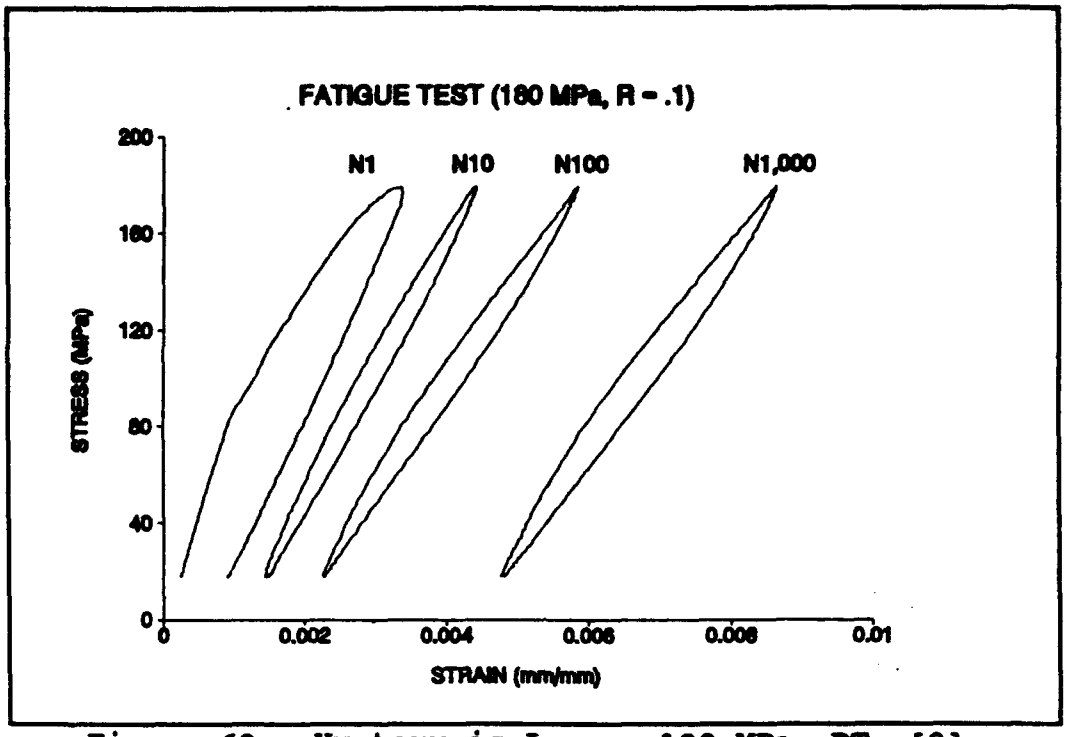

Figure 69. Hysterysis Loops, 180 MPa, RT, [8].

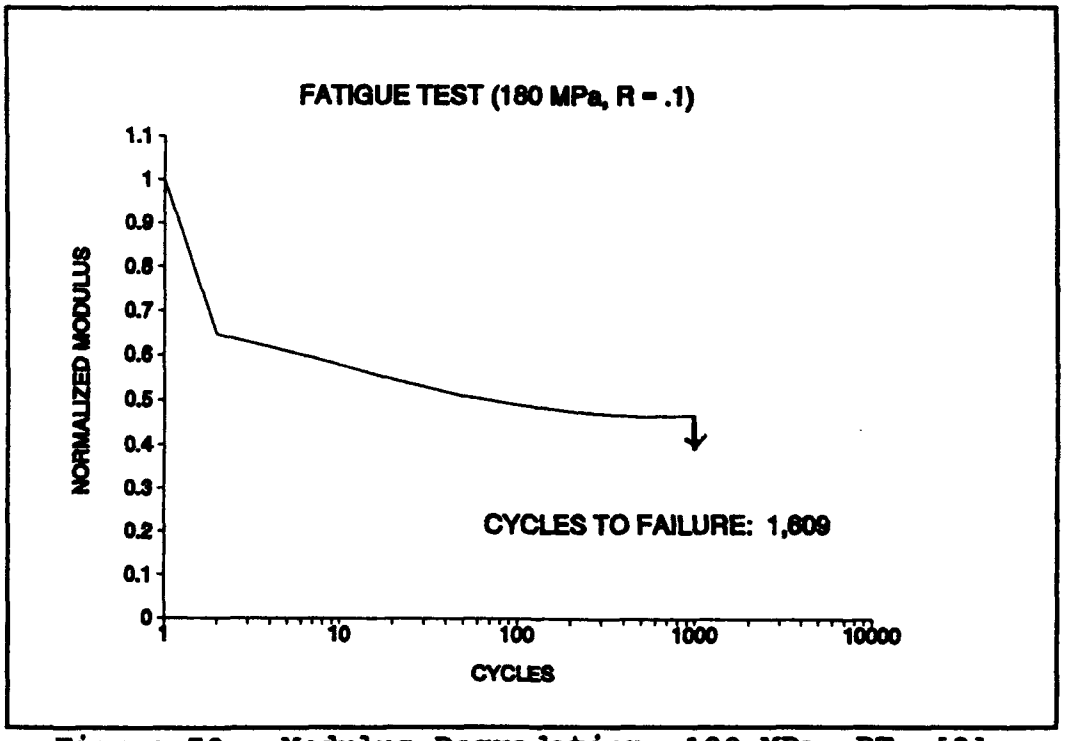

Figure 70. Modulus Degradation, 180 MPa, RT, [8].

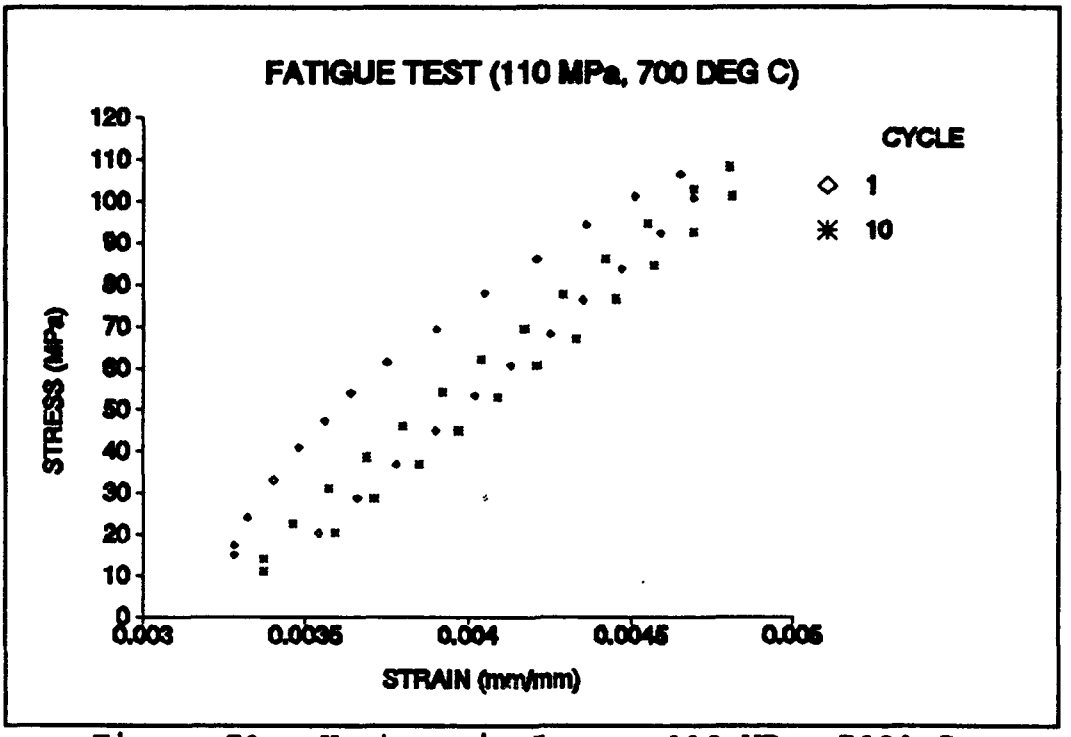

Figure 71. Hysterysis Loops, 110 MPa, 700° C.

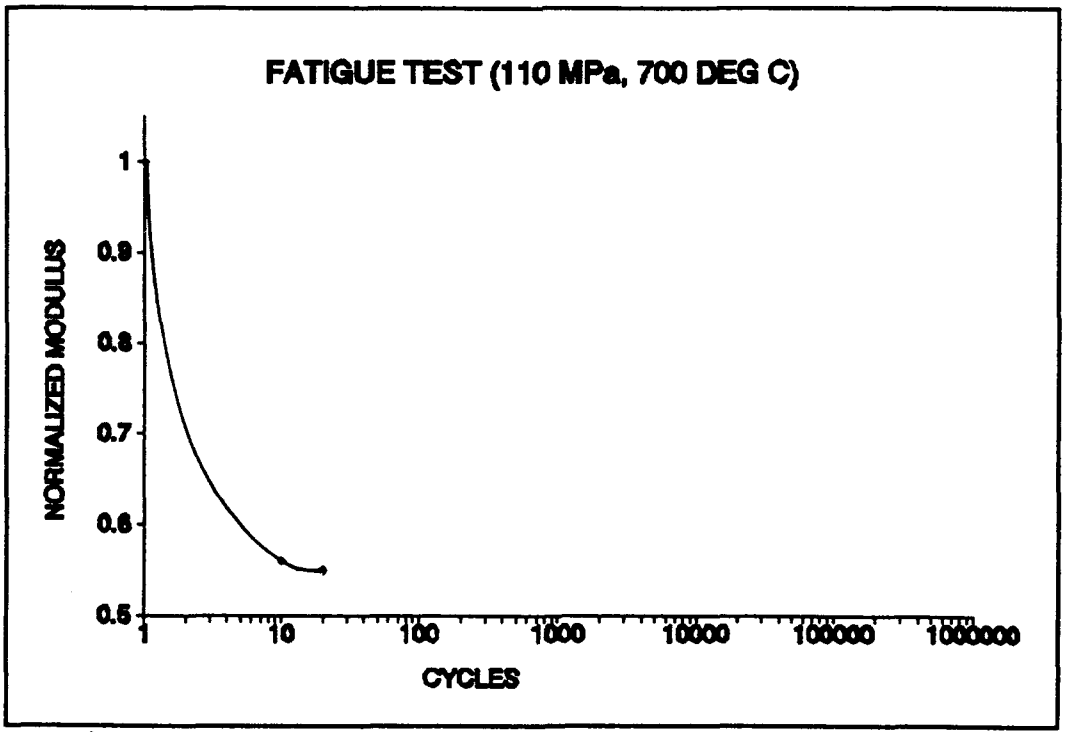

Figure 72. Modulus Degradation, 110 MPa, 700° C.

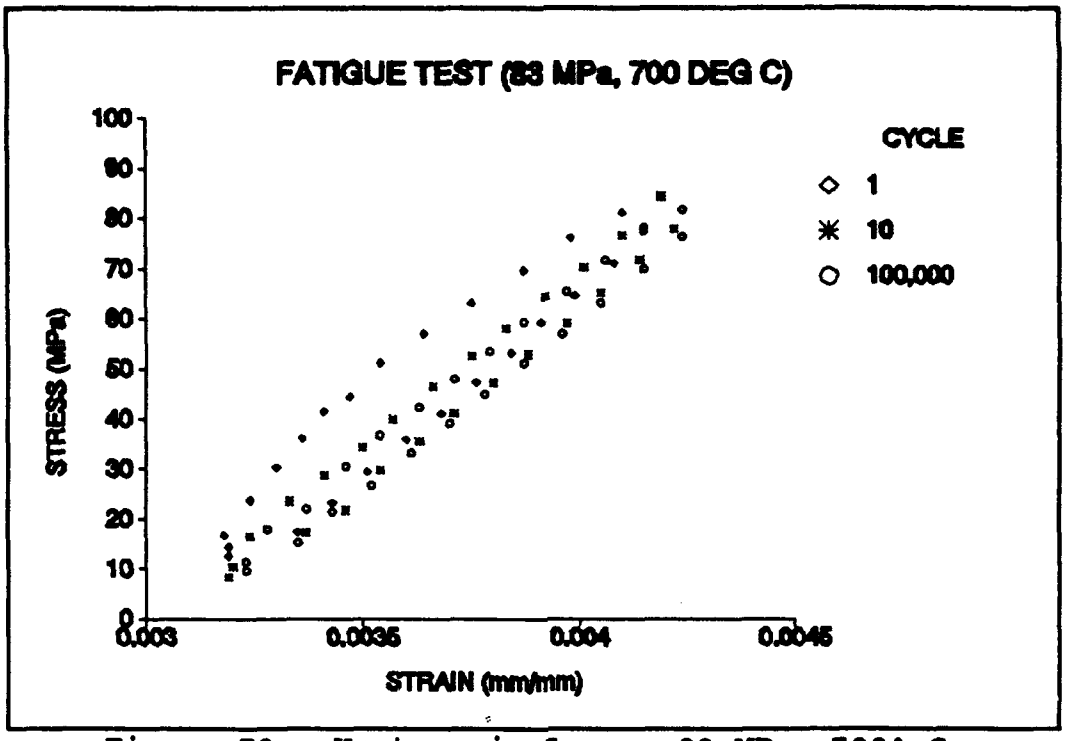

Figure 73. Hysterysis Loops, 83 MPa, 700° C.

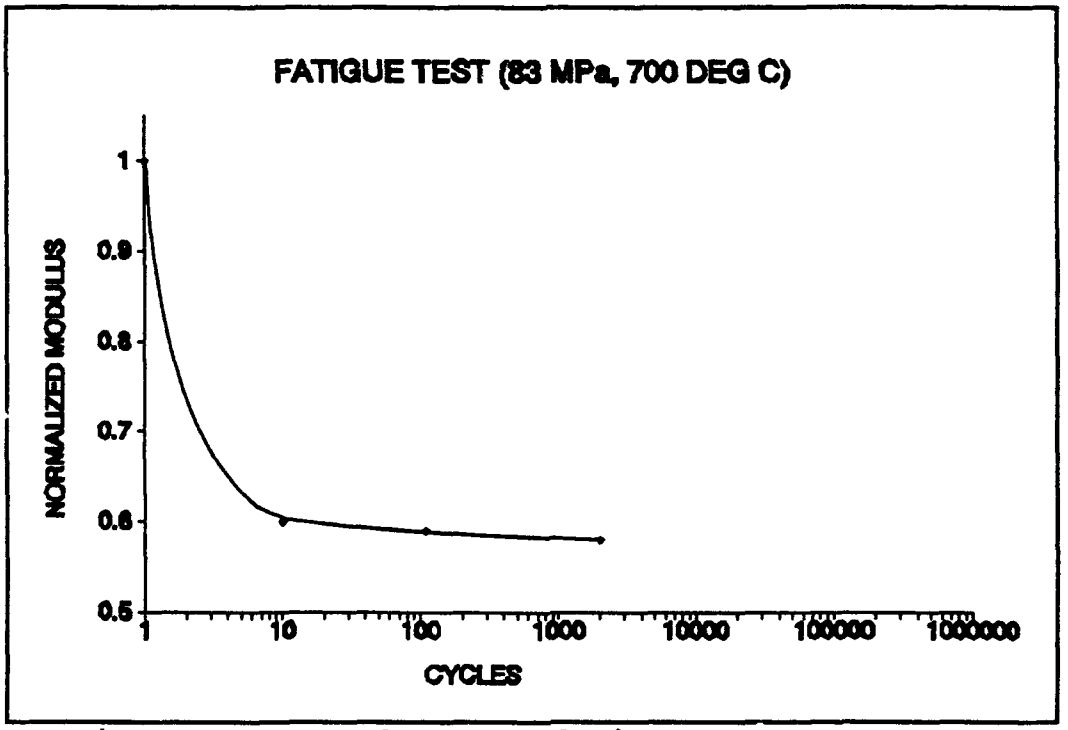

Figure 74. Modulus Degradation, 83 MPa, 700° C.

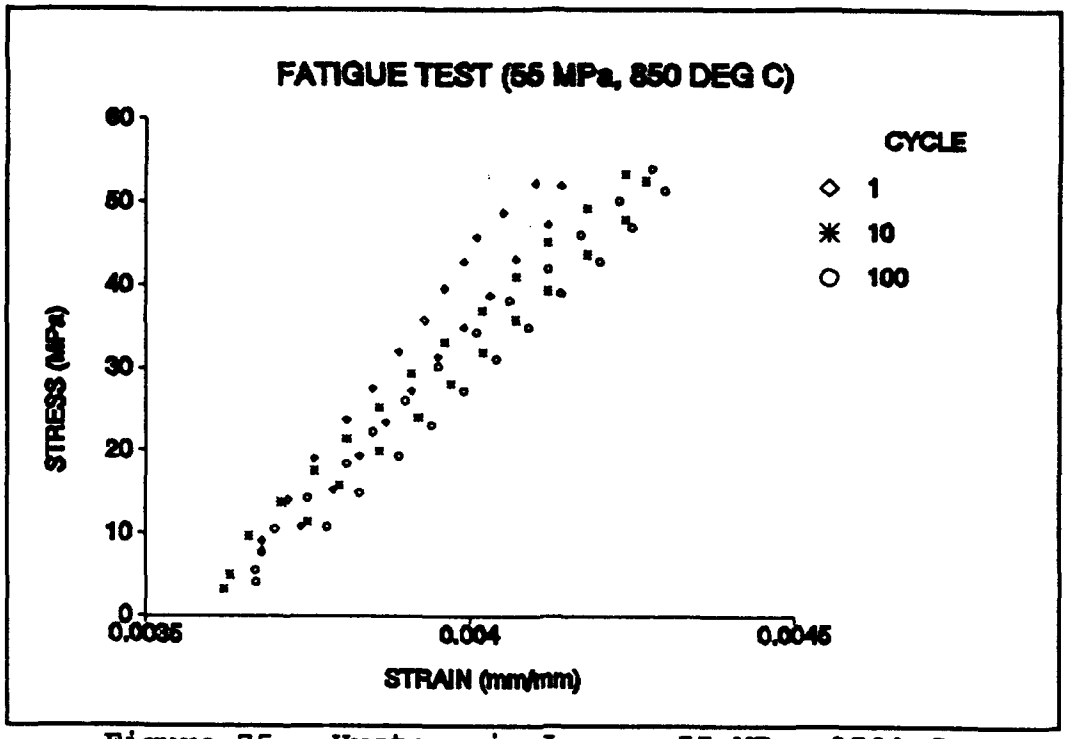

Figure 75. Hysterysis Loops, 55 MPa, 850° C.

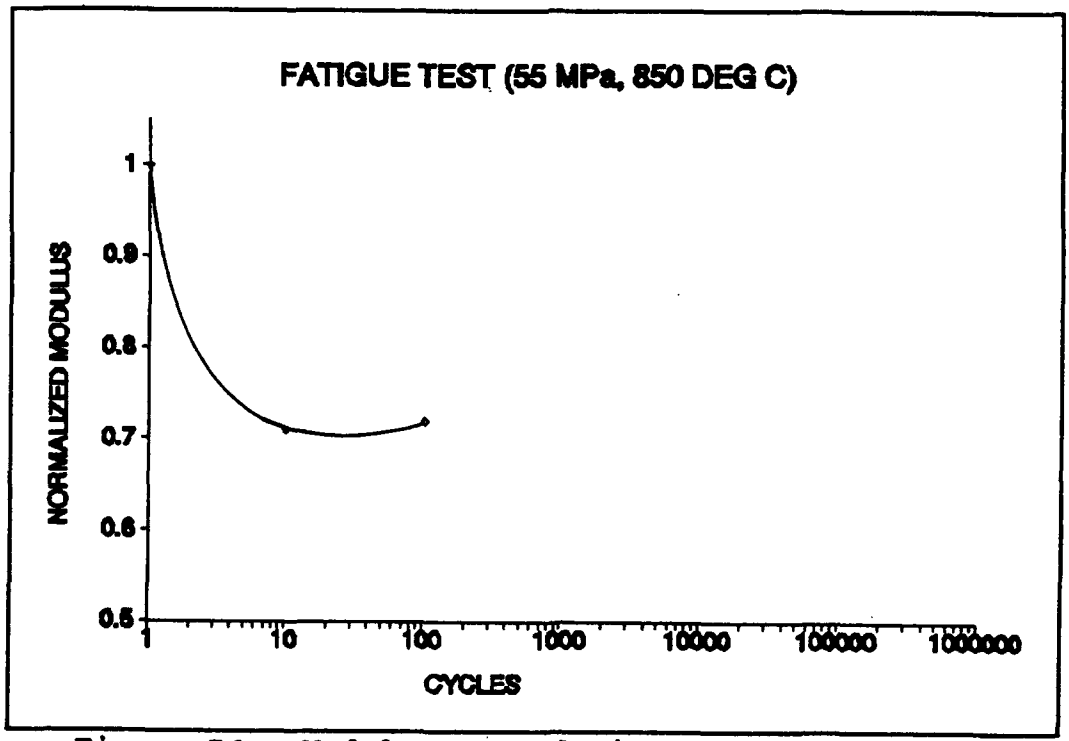

Figure 76. Modulus Degradation, 55 MPa, 850° C.

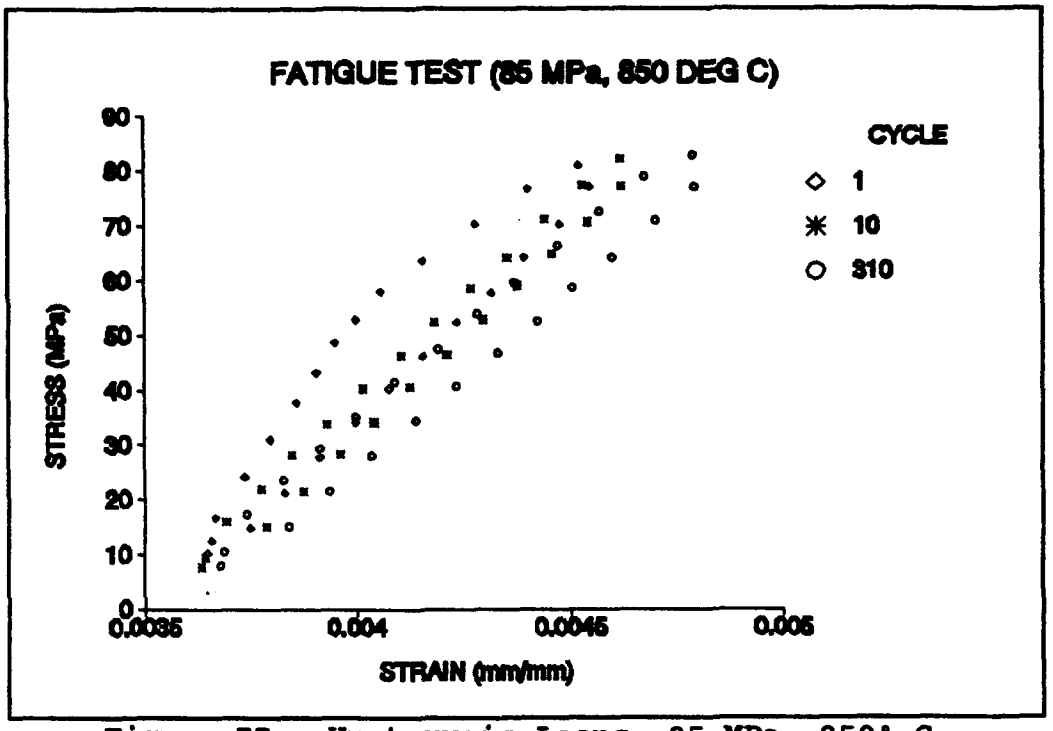

Figure 77. Hysterysis Loops, 85 MPa, 850° C.

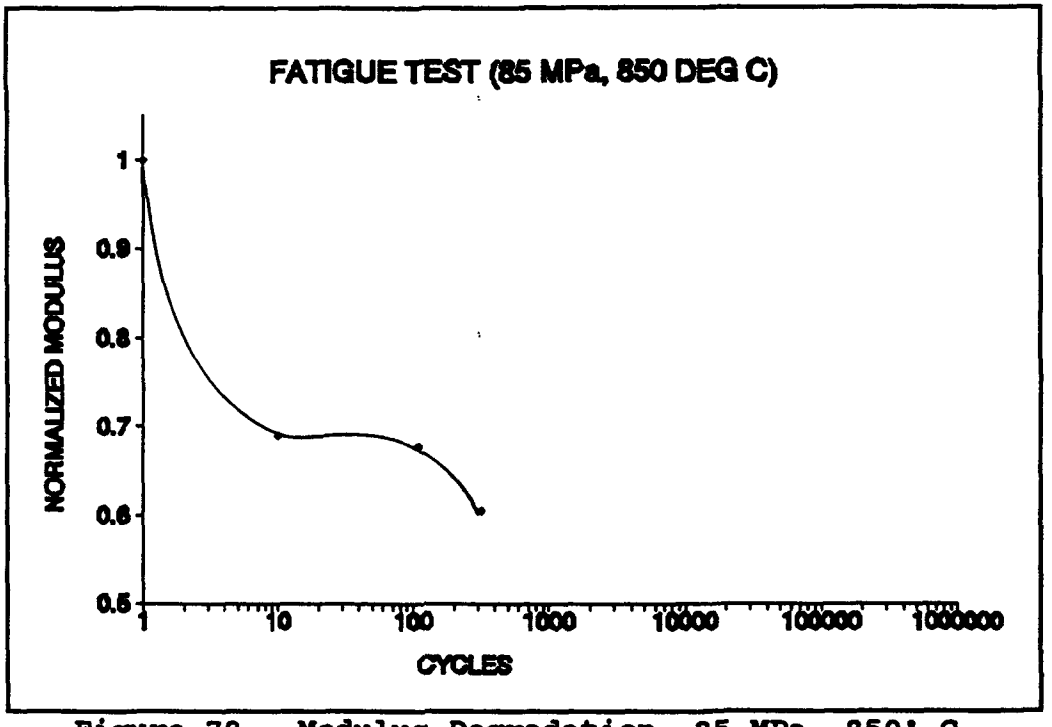

Figure 78. Modulus Degradation, 85 MPa, 850° C.

Vita

Captain Richard J. Tuznik was born in Detroit, Michigan. He graduated from Notre Dame High School, Harper Woods, Michigan in 1977. He enlisted in the United States Air Force in 1980 and completed the Ground Radio Communications Equipment Repairman Technical Training Course.

In 1985, then Staff Sergeant Tuznik earned an Associate in Applied Science Degree With the Community College of the Air Force. He was selected as the Air Force Communications Command Technician/Supervisor of the Year. He was also selected to participate in the Airman's Education and Commissioning Program.

He graduated from Oklahoma State University, Stillwater, Oklahoma in 1989 with a Bachelor of Science Degree in Mechanical Engineering. He was commissioned after completing Officer Training School. He entered the School of Engineering, Air Force Institute of Technology in May of 1992.

Captain Tuznik's military decorations include the Air Force Commendation Medal with one oak leaf cluster and the Air Force Achievement Medal with one oak leaf cluster.

REPORT DOCUMENTATION PAGE

Form Approved
OMB No. 0704-0188

1. AGENCY USE ONLY *(Leave blank)*	2. REPORT DATE	3. REPORT TYPE AND DATES COVERED
	December 1993	Masters Thesis

4. TITLE AND SUBTITLE
FATIGUE BEHAVIOR OF A CROSS-PLY CERAMIC MATRIX COMPOSITE AT ELEVATED TEMPERATURES UNDER TENSION-TENSION LOADING

5. FUNDING NUMBERS

6. AUTHOR(S)

7. PERFORMING ORGANIZATION NAME(S) AND ADDRESS(ES)

Air Force Institute of Technology
WPAFB OH 45433-7765

8. PERFORMING ORGANIZATION REPORT NUMBER

AFIT/GAE/ENY/93D-28

9. SPONSORING/MONITORING AGENCY NAME(S) AND ADDRESS(ES)

Dr. Walter Jones
AFOSR/NA
Bolling AFB, DC 20322-6448

10. SPONSORING/MONITORING AGENCY REPORT NUMBER

11. SUPPLEMENTARY NOTES

12a. DISTRIBUTION/AVAILABILITY STATEMENT

Approved for public release; distribution unlimited

12b. DISTRIBUTION CODE

13. ABSTRACT *(Maximum 200 words)*

A study was conducted which investigated the behavior of a Nicalon/Calcium-Aluminosilicate (Nicalon/CAS) cross-ply ($[0/90]_{2S}$) ceramic matrix composite at elevated temperatures under tension-tension fatigue loading. Tension-tension fatigue tests were performed with a load ratio of R = 0.10 and a frequency of 10 Hertz at 700°C and 850°C. These results were compared to results from a previous study conducted at room temperature. Material behavior and damage was recorded by fatigue life curves, elastic modulus, maximum and minimum strain, acetate replication techniques, and post-mortem fractography. Analysis of these results showed identical matrix dominated damage behavior at RT and 700°C. Ultimate failure was caused by an accumulation of matrix damage, most of which occurred on the first cycle. However, at 850°C, significantly less damage occurred to the matrix and failure was fiber dominated. Fiber debonding was identified as the major damage mechanism responsible for final failure at this elevated temperature.

14. SUBJECT TERMS	15. NUMBER OF PAGES
Ceramic Matrix Composite, Tension-Tension Fatigue Elevated Temperature, Fiber Debonding	97
	16. PRICE CODE

17. SECURITY CLASSIFICATION OF REPORT	18. SECURITY CLASSIFICATION OF THIS PAGE	19. SECURITY CLASSIFICATION OF ABSTRACT	20. LIMITATION OF ABSTRACT
Unclassified	Unclassified	Unclassified	UL